

# Ensemble Transport Filter via Optimized Maximum Mean Discrepancy \*

Dengfei Zeng<sup>†</sup> and Lijian Jiang<sup>‡</sup>

**Abstract.** In this paper, we present a new ensemble-based filter method by reconstructing the analysis step of the particle filter through a transport map, which directly transports prior particles to posterior particles. The transport map is constructed through an optimization problem described by the Maximum Mean Discrepancy loss function, which matches the expectation information of the approximated posterior and reference posterior. The proposed method inherits the accurate estimation of the posterior distribution from particle filtering. To improve the robustness of Maximum Mean Discrepancy, a variance penalty term is used to guide the optimization. It prioritizes minimizing the discrepancy between the expectations of highly informative statistics for the approximated and reference posteriors. The penalty term significantly enhances the robustness of the proposed method and leads to a better approximation of the posterior. A few numerical examples are presented to illustrate the advantage of the proposed method over ensemble Kalman filter.

**Key words.** Ensemble Assimilation method, Transport Map, Maximum Mean Discrepancy

**1. Introduction.** Data assimilation aims to obtain a reliable state estimate of the dynamical system by best combining observations and mathematical models [16, 19, 23]. The development of data assimilation provides powerful tools for applications in many fields, such as geophysics, atmosphere science, and numerical weather prediction [1, 10, 14, 33]. The filtering method is an important class of sequence data assimilation technique. In the Bayesian framework, the main procedure of filtering consists of two steps: the prediction step and the analysis step. The prediction step gives prior information based on the numerical simulation of the transition model, and the analysis step solves a Bayesian inverse problem based on the Bayes' rule conditioned on given observations.

The main challenge of the filtering method lies in the analysis step because it is difficult to accurately estimate the posterior distribution when the dynamical system is characterized by a high dimensional state space [3, 34], strong nonlinearly transition and observation operator [15, 20], and sparse observations [28]. A theoretical analysis of optimal nonlinear filtering is investigated in [17, 18]. The optimal mean square estimate in filtering is equivalent to the posterior mean. However, it is difficult to determine the exact posterior without particular assumptions on the structure of the filter problem. The ensemble Kalman filter (EnKF) is the most popular data assimilation method for nonlinear systems, which gives a sub-optimal state estimation for weakly nonlinear systems based on Gaussian assumptions [6, 7, 8]. However, the EnKF ignores the inconsistency of the sensitivity of each particle under a strongly nonlinear system [27]. Moreover, due to its Gaussian assumption, it can not correctly approximate the non-

---

\*L. Jiang acknowledges the support of NSFC 12271408.

<sup>†</sup>School of Mathematical Sciences, Tongji University, Shanghai 200092, China. (dfzeng@tongji.edu.cn).

<sup>‡</sup>School of Mathematical Sciences, Tongji University, Shanghai 200092, China. (ljjiang@tongji.edu.cn), Corresponding author.

Gaussian prior distribution of the state, which significantly limits the application of the EnKF [21]. Another well-known filtering method is particle filtering (PF), which is a Monte Carlo method based on sequential importance sampling. In the asymptotic sense, the posterior approximated by PF converges to the true posterior of the data assimilation problem as the number of particles increases to infinity [9, 16]. However, PF suffers from the curse of dimensionality, which often manifests as particle collapse in sequence updating. The number of particles required in PF grows exponentially with respect to the dimension of state space [2]. Resampling can alleviate the challenge by resetting the particle weights to be the same, but it is often not enough to offset this shortcoming. Local particle filtering methods incorporate the concept of localization into particle filtering, which reduces the risk of particle collapse [25, 29]. However, it is challenging to effectively and consistently merge the locally updated particles.

Although Bayesian filtering methods have different forms, they define explicit or implicit transport maps, which push forward the prior distribution to the posterior distribution based on different assumptions on the prior distribution and the likelihood function. The idea of transferring probability measures through a transport map has been well-developed and has been widely used in fluid dynamics, economics, statistics, machine learning, and many other fields [5, 22, 30]. In recent years, the study of transport has gained much attention to treat the challenges of data assimilation in high-dimensional and non-Gaussian nonlinear systems. Some suitable transport maps can be constructed by optimizing the KL divergence between the distribution of the prior and the distribution corresponding to the inverse transport map of the posterior. Spanini et al., [28], proposed an ensemble filtering method based on the coupling technique and obtained a non-Gaussian extension of the ensemble Kalman filter by constructing the Knothe-Rosenblatt rearrangement. Pulido et al., [23], construct a sequence of kernel embedded mappings that represent a gradient flow based on the principles of local optimal transport. Hoang et al., [13], incorporated machine learning into the conditional mean filter and got a nonlinear transformation based on the condition mean’s orthogonal projection property.

In this paper, we propose a transport map that directly transports the prior particles to the posterior particles by reconstructing the PF analysis step. Unlike implicit sampling filtering methods [4, 34], we convert the construction of the transport map into an optimization problem for the Maximum Mean Discrepancy (MMD) loss function by matching the moment information of the approximated posterior generated by transport map and the posterior of PF. In this way, the weight information of the analysis step of PF is converted into updates of the particle states. The proposed method is called as an ensemble transport filter. Here, we take the function space of MMD as a Reproducing Kernel Hilbert Space (RKHS), and then the MMD can be calculated with kernel function in a simplified way. When the kernel function is a universal kernel, it ensures that the distribution obtained through the transport map converges to the reference posterior given by PF as the MMD loss tends to zero. To enhance the robustness of MMD in handling high-dimensional state space [24], we introduce a penalty term

based on the variances of the source and target distributions to push the method to prioritize minimizing the mean discrepancy on highly informative statistics. The variance penalty term effectively enhances the robustness of our method in approximating the filtering posterior, making it more effective and stable. Numerical examples show that the ensemble transport filter with a variance penalty term significantly improves robustness in high-dimensional and non-Gaussian problems.

The rest of the article is organized as follows. In [section 2](#), we introduce the nonlinear filtering problem of a stochastic dynamical system and build a connection with the transfer of distributions. The transport map is constructed in [section 3](#) by optimizing the mean discrepancy between the approximated posterior and reference posterior. To enhance the robustness of MMD, a variance penalty term is introduced. Numerical examples are presented to evaluate the performance of the ensemble transport filter in [section 4](#). Finally, we briefly conclude this article in [section 5](#).

**2. Bayesian formulation of nonlinear filter.** This section reviews the nonlinear filtering problem of stochastic dynamical systems. Then we reformulate the filtering process as a transfer from prior distribution to posterior distribution.

**2.1. State estimation of dynamical system.** Consider the continuous-time dynamical model

$$d\mathbf{X}_t = \mathcal{M}(\mathbf{X}_t)dt + d\mathbf{N}_x,$$

where the model noise  $\mathbf{N}_x$  is a  $\mathbb{R}^n$ -valued stochastic process. Most often,  $\mathbf{N}_x$  is set to be a Brownian motion, but sometimes Levy processes are used to account for non-Gaussian noise [28]. The system is discretized in time for simulation. Suppose the discrete stepsize of time is  $\Delta t$ , we get  $\mathbf{X}_{(k)\Delta t} = \mathbf{X}_{(k-1)\Delta t} + \mathcal{M}(\mathbf{X}_{(k-1)\Delta t})\Delta t + \Delta\mathbf{N}_x$  with Euler-Maruyama scheme[12]. This leads to a discrete stochastic dynamical model,

$$(2.1) \quad \mathbf{X}_k = \mathcal{M}_k(\mathbf{X}_{k-1}) + \boldsymbol{\eta}_k,$$

where  $\mathcal{M}_k$  is the transition model and  $\boldsymbol{\eta}_k$ , with  $k = \{0, 1, 2, \dots\}$ , are the model noise that is assumed to be statistical independent. Noisy observations of state  $\mathbf{x}_k$  are available at discrete times

$$(2.2) \quad \mathbf{Y}_k = \mathcal{H}_k(\mathbf{x}_k) + \boldsymbol{\epsilon}_k.$$

where  $\mathcal{H} : \mathbb{R}^m \rightarrow \mathbb{R}^n$  is the observation operator and  $\boldsymbol{\epsilon}_k$  is the observation noise.

The discrete representation of dynamical model (2.1) and observation operator (2.2) can be seen as a state-space model. [Figure 1](#) shows the directed probability graph of state space model. With the assumed random nature of both model and observation noise, the model states and observations can be described as random variables. Filtering aims to infer the conditional posterior  $\pi_{\mathbf{X}_k|\mathbf{Y}_{1:k}}$  sequentially, and then a Bayesian framework can be used.

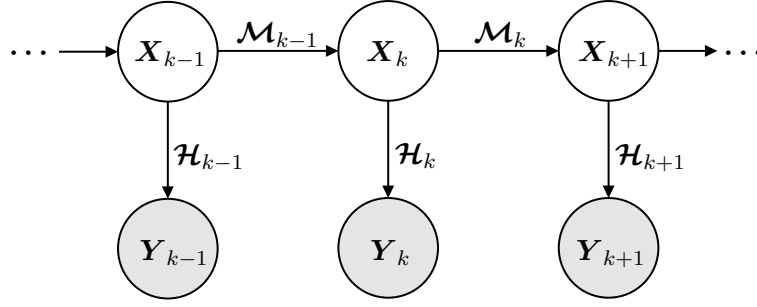


**Figure 1.** Directed probability graph of dynamical model (2.1) and observation operator (2.2) in the form of state-space model

**2.2. Sequential Bayesian Filtering.** Define the sequence of model states and observations by  $\mathbf{x}_{0:K} = \{\mathbf{x}_0, \mathbf{x}_1, \dots, \mathbf{x}_K\}$  and  $\mathbf{y}_{0:K} = \{\mathbf{y}_1, \mathbf{y}_2, \dots, \mathbf{y}_K\}$ , respectively. The procedure of sequential Bayesian filtering is to estimate the  $\pi_{\mathbf{X}_k | \mathbf{Y}_{1:k}}$  iteratively. Assuming the prior of the initial state  $\mathbf{X}_0$  to be  $\pi_{\mathbf{X}_0}$ , the sequential Bayesian filtering of the state-space model consists of two steps: forecast and analysis.

- **Forecast:** estimate the prior distribution of iteration step  $k$  with the Chapman-Kolmogorov equation

$$(2.3) \quad \pi_{\mathbf{X}_k | \mathbf{Y}_{1:k-1}} = \int \pi_{\mathbf{X}_k | \mathbf{X}_{k-1}} \pi_{\mathbf{X}_{k-1} | \mathbf{Y}_{1:k-1}} d\mathbf{X}_{k-1},$$

where  $\pi_{\mathbf{X}_k | \mathbf{X}_{k-1}}$  is the transition probability.

- **Analysis:** update the conditional posterior distribution at iteration step  $k$  based on Bayes' rule

$$(2.4) \quad \pi_{\mathbf{X}_k | \mathbf{Y}_{1:k}} = \frac{\pi_{\mathbf{X}_k | \mathbf{Y}_{1:k-1}} \pi_{\mathbf{Y}_k | \mathbf{X}_k}}{\pi_{\mathbf{Y}_k | \mathbf{Y}_{1:k-1}}},$$

where  $\pi_{\mathbf{Y}_k | \mathbf{X}_k}$  is the observation likelihood and  $\pi_{\mathbf{Y}_k | \mathbf{Y}_{1:k-1}}$  is the marginal likelihood given by

$$\pi_{\mathbf{Y}_k | \mathbf{Y}_{1:k-1}} = \int \pi_{\mathbf{X}_k | \mathbf{Y}_{1:k-1}} \pi_{\mathbf{Y}_k | \mathbf{X}_k} d\mathbf{X}_k.$$

The integral of Chapman-Kolmogorov equation (2.3) and marginal likelihood  $\pi_{\mathbf{Y}_k | \mathbf{Y}_{1:k-1}}$  of (2.4) can not be calculated analytically in general settings. To overcome this difficulty, an ensemble of particles are used to represent the uncertainty of states and observations in ensemble-based filters. In ensemble-based filters, the filtering process involves transporting particles between three related probability distributions (see Figure 2).

In the forecast step, the transition density  $\pi_{\mathbf{X}_k | \mathbf{X}_{k-1}}$  is given by a dynamical model, such as like (2.1). By an ensemble of particles  $\{\mathbf{x}_{k-1}^{(i)}\}_{i=1}^N$  drawn from posterior distribution  $\pi_{\mathbf{X}_{k-1} | \mathbf{Y}_{1:k-1}}$  of the previous time step, we can sample exactly from transition density  $\pi_{\mathbf{X}_k | \mathbf{X}_{k-1}}$  via the discrete dynamical model (2.1). Thus, the generated particles  $\{\hat{\mathbf{x}}_k^{(i)}\}_{i=1}^N$  can be regarded as samples drawn from prior distribution  $\pi_{\mathbf{X}_k | \mathbf{Y}_{1:k-1}}$  of

the current time step. Given the likelihood function and prior distribution approximated by the ensemble of particles, the main task of the analysis step is to seek an approximation of posterior distribution at the current time step. EnKF and its variants approximate the posterior distribution with an ensemble of particles generated from a linear transformation of prior particles under a Gaussian ansatz on prior [27]. Particle filter changes the weights of prior particles through the likelihood function to obtain an accurate estimate of the posterior distribution without altering the state of the prior particles, and a resampling procedure is used to normalize weights [2].

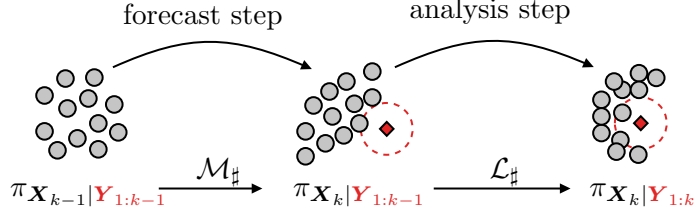


**Figure 2.** Propagation of particles between distributions in ensemble-based filtering

For the convenience of presentation, we denote  $\hat{\mathbf{X}}_k$  as the random variable of forecast distribution  $\pi_{\mathbf{X}_k|\mathbf{Y}_{1:k-1}}$ . From the point of view of transport, the ensemble-based filter has two transport processes of distribution, which are denoted as push-forward operators  $\mathcal{M}_{\#}$  and  $\mathcal{L}_{\#}$  shown in Figure 2. The  $\mathcal{M}_{\#}$  and  $\mathcal{L}_{\#}$  define the transition probability  $\pi_{\mathbf{X}_k|\mathbf{X}_{k-1}}$  and  $\pi_{\mathbf{X}_k|\hat{\mathbf{X}}_k, \mathbf{Y}_k}$ , respectively,

$$(2.5) \quad \pi_{\hat{\mathbf{X}}_k} = \int \pi_{\hat{\mathbf{X}}_k|\mathbf{X}_{k-1}} \pi_{\mathbf{X}_{k-1}|\mathbf{Y}_{1:k-1}} d\mathbf{X}_{k-1} = \mathcal{M}_{\#} \pi_{\mathbf{X}_{k-1}|\mathbf{Y}_{1:k-1}},$$

$$(2.6) \quad \pi_{\mathbf{X}_k|\mathbf{Y}_{1:k}} = \int \pi_{\mathbf{X}_k|\hat{\mathbf{X}}_k, \mathbf{Y}_k} \pi_{\hat{\mathbf{X}}_k} d\hat{\mathbf{X}}_k = \mathcal{L}_{\#} \pi_{\hat{\mathbf{X}}_k}.$$

Different ensemble filtering methods provide approximate alternatives to the transition probability for the analysis step through different transport maps of ensemble particles. EnKF explicitly constructs a linear transport map, which performs efficiently and robustly in linear and weakly nonlinear systems but performs poorly in strongly nonlinear systems. On the other hand, the particle filter can be viewed as an implicit transport map, providing exact filtering but susceptible to particle degeneracy, thus suffering from the curse of dimensionality. In this article, we intend to obtain an approximation of transition probabilities  $\pi_{\mathbf{X}_k|\hat{\mathbf{X}}_k, \mathbf{Y}_k}$  by constructing an explicit transport map which reconstructs the analysis step of the particle filter.

**3. Ensemble Transport Filter.** In this section, a transport map is constructed to approximate the transition probability for the analysis step. In subsection 3.1, we formulate the construction as an optimization task on a Maximum Mean Discrepancy loss by matching the posterior expectation. The algorithm of the ensemble-based transport filter is presented in subsection 3.2. Finally, in subsection 3.3, a variance penalty is

introduced to improve the robustness of MMD. Moreover, a linear transport filter is derived, and it shares the similar form to EnKF.

**3.1. Proposal transition generated by transport map in analysis step.** In filtering, we typically use the posterior mean as the state estimate. Here, we start by considering the posterior mean of an arbitrary function  $f \in \mathcal{C}(\mathbb{R}^n)$ . For simplicity, we suppress the subscripts of the probability density functions in the derivation.

$$\begin{aligned}
\mathbb{E}_{\pi_{\mathbf{x}_k|\mathbf{Y}_{1:k}}} [f(\mathbf{x}_k)] &= \int f(\mathbf{x}_k) \pi(\mathbf{x}_k | \mathbf{y}_{1:k}) d\mathbf{x}_k \\
(3.1) \quad &= \frac{1}{A} \int f(\mathbf{x}_k) \pi(\mathbf{y}_k | \mathbf{x}_k) \pi(\mathbf{x}_k | \mathbf{y}_{1:k-1}) d\mathbf{x}_k \\
&= \frac{1}{A} \int f(\mathbf{x}_k) \pi(\mathbf{y}_k | \mathbf{x}_k) \pi(\mathbf{x}_k | \mathbf{x}_{k-1}) \pi(\mathbf{x}_{k-1} | \mathbf{y}_{1:k-1}) d\mathbf{x}_k d\mathbf{x}_{k-1},
\end{aligned}$$

in which Bayes' theorem and Chapman-Kolmogorov equation are used, and  $A$  is a normalization factor.

In the particle filter, the posterior distribution at the previous time step can be approximated by the summation of Dirac-delta centered at particles with equal weights, i.e.,

$$(3.2) \quad \pi(\mathbf{x}_{k-1} | \mathbf{y}_{1:k-1}) \approx \frac{1}{N} \sum_{i=1}^N \delta_{\mathbf{x}_{k-1}^{(i)}}(\mathbf{x}_{k-1}).$$

Then, the samples of forecast distribution  $\pi_{\mathbf{x}_k|\mathbf{Y}_{1:k-1}}$  can be drawn from the transition density  $\pi(\mathbf{x}_k | \mathbf{x}_{k-1})$  via the discrete dynamical model (2.1), which gives  $\{\hat{\mathbf{x}}_k^{(i)}\}_{i=1}^N$ . Filtering prior distribution at time step  $k$  can be estimated by

$$(3.3) \quad \pi(\mathbf{x}_k | \mathbf{y}_{1:k-1}) \approx \frac{1}{N} \sum_{i=1}^N \delta_{\hat{\mathbf{x}}_k^{(i)}}(\mathbf{x}_k).$$

Observations are introduced through particle weights computed with the likelihood function. The posterior expectation of function  $f(\mathbf{x})$  can be estimated by

$$(3.4) \quad \mathbb{E}_{\pi_{\mathbf{x}_k|\mathbf{Y}_{1:k}}} [f(\mathbf{x}_k)] \approx \sum_{i=1}^N w_i f(\hat{\mathbf{x}}_k^i), \quad w_i = \frac{\pi(\mathbf{y}_k | \hat{\mathbf{x}}_k^{(i)})}{\sum_{j=1}^N \pi(\mathbf{y}_k | \hat{\mathbf{x}}_k^{(j)})}.$$

Combining (2.5)-(2.6), the posterior expectation (3.1) can also be represented by

$$\mathbb{E}_{\pi_{\mathbf{x}_k|\mathbf{Y}_{1:k}}} [f(\mathbf{x}_k)] = \int f(\mathbf{x}_k) \pi(\mathbf{x}_k | \hat{\mathbf{x}}_k, \mathbf{y}_k) \pi(\hat{\mathbf{x}}_k | \mathbf{x}_{k-1}) \pi(\mathbf{x}_{k-1} | \mathbf{y}_{1:k-1}) d\hat{\mathbf{x}}_k d\mathbf{x}_{k-1} d\mathbf{x}_k.$$

As discussed in subsection 2.2, the transition probability density  $\pi_{\mathbf{x}_k|\hat{\mathbf{x}}_k,\mathbf{Y}_k}$  is implicitly defined through the likelihood function. Here, we find a transition probability density

$q_{\mathbf{X}_k|\hat{\mathbf{X}}_k,\mathbf{y}_k}^{\mathcal{T}_k}$  through a parametric transport map  $\mathcal{T}_k$  to obtain particles from the posterior distribution directly. To eliminate the intermediate variable  $\hat{\mathbf{X}}_k$ , we denote

$$q^{\mathcal{T}_k}(\mathbf{x}_k | \mathbf{x}_{k-1}, \mathbf{y}_k) = \int q^{\mathcal{T}_k}(\mathbf{x}_k | \hat{\mathbf{x}}_k, \mathbf{y}_k) \pi(\hat{\mathbf{x}}_k | \mathbf{x}_{k-1}) d\hat{\mathbf{x}}_k.$$

Insert  $q^{\mathcal{T}_k}(\mathbf{x}_k | \mathbf{x}_{k-1}, \mathbf{y}_k)$  into (3.1), we can rewrite it as

$$(3.5) \quad \mathbb{E}_{\pi_{\mathbf{x}_k|\mathbf{y}_{1:k}}} [f(\mathbf{x}_k)] = \int f(\mathbf{x}_k) h^{\mathcal{T}_k}(\mathbf{x}_{k-1:k}, \mathbf{y}_k) q^{\mathcal{T}_k}(\mathbf{x}_k | \mathbf{x}_{k-1}, \mathbf{y}_k) \pi(\mathbf{x}_{k-1} | \mathbf{y}_{1:k-1}) d\mathbf{x}_k d\mathbf{x}_{k-1},$$

where  $h^{\mathcal{T}_k}(\mathbf{x}_{k-1:k}, \mathbf{y}_k) = \frac{\pi(\mathbf{y}_k|\mathbf{x}_k)\pi(\mathbf{x}_k|\mathbf{x}_{k-1})}{Aq^{\mathcal{T}_k}(\mathbf{x}_k|\mathbf{x}_{k-1},\mathbf{y}_k)}$ .

If a transport map  $\mathcal{T}_k$  is selected, the transition probability density  $q_{\mathbf{X}_k|\hat{\mathbf{X}}_k,\mathbf{y}_k}^{\mathcal{T}_k}$  corresponding to the map satisfy

$$(3.6) \quad h^{\mathcal{T}_k}(\mathbf{x}_{k-1:k}, \mathbf{y}_k) \equiv 1.$$

Thus, we obtain a transport map that transports the prior samples to the posterior samples. The posterior expectation of function  $f(\mathbf{x})$  can be estimated by

$$\mathbb{E}_{\pi_{\mathbf{x}_k|\mathbf{y}_{1:k}}} [f(\mathbf{x}_k)] \approx \frac{1}{N} \sum_{i=1}^N f(\mathcal{T}_k(\mathbf{x}_k^{(i)})).$$

It is difficult to directly solving (3.6) because the normalization constant  $A$  is inaccessible. We can not obtain an analytical form for the transition probability corresponding to the nonlinear transport map. However, we can compute  $\mathcal{T}_k$  indirectly. In a compact form, we can use the Chapman-Kolmogorov formula to obtain an approximated posterior probability density,

$$q^{\mathcal{T}_k}(\mathbf{x}_k | \mathbf{y}_{1:k}) = \int q^{\mathcal{T}_k}(\mathbf{x}_k | \mathbf{x}_{k-1}, \mathbf{y}_k) \pi(\mathbf{x}_{k-1} | \mathbf{y}_{1:k-1}) d\mathbf{x}_{k-1}.$$

If the approximated posterior  $q^{\mathcal{T}_k}(\mathbf{x}_k | \mathbf{y}_{1:k})$  is equal to the true posterior, the desired transport map  $\mathcal{T}_k$  is found.

**Lemma 3.1.** (Lemma 9.3.2 in [26]) *Let  $(\Omega, d)$  be a metric space, and  $p, q$  be two probability measure defined on  $\Omega$ . Then  $p = q$  if and only if  $\mathbb{E}_{\mathbf{x} \sim p}[f(\mathbf{x})] = \mathbb{E}_{\mathbf{y} \sim q}[f(\mathbf{y})]$  for all  $f \in \mathcal{C}(\Omega)$ , where  $\mathcal{C}(\Omega)$  is the space of bounded continuous on  $\Omega$ .*

The following proposition is a direct result of Lemma 3.1, and it proves that the resulting posterior probability density gives an approximation of the true posterior probability density under certain conditions.

**Proposition 3.2.** *Given transport map  $\mathcal{T}_k : \mathbb{R}^n \rightarrow \mathbb{R}^n$ , the transition probability density  $q_{\mathbf{X}_k|\hat{\mathbf{X}}_k,\mathbf{y}_k}^{\mathcal{T}_k}$  corresponds to transport map  $\mathcal{T}_k$  generates the posterior  $q_{\mathbf{X}_k|\mathbf{Y}_{1:k}}^{\mathcal{T}_k}$ . If the expectation of posterior and true posterior are matched for all  $f \in \mathcal{C}(\mathbb{R}^n)$ ,*

$$\int f(\mathbf{x}_k)\pi(\mathbf{x}_k | \mathbf{y}_{1:k})d\mathbf{x}_k = \int f(\mathbf{x}_k)q^{\mathcal{T}_k}(\mathbf{x}_k | \mathbf{y}_{1:k})d\mathbf{x}_k,$$

*then the approximated posterior  $q^{\mathcal{T}_k}(\mathbf{x}_k | \mathbf{y}_{1:k})$  is identical to the true posterior.*

Based on [Proposition 3.2](#), we can reformulate the problem of finding transport map  $\mathcal{T}_k$  as the optimization problem,

$$(3.7) \quad \mathcal{T}_k = \arg \min_{\mathcal{S}} \sup_{f \in \mathcal{C}(\mathbb{R}^n)} \left( \mathbb{E}_{\mathbf{x} \sim \pi_{\mathbf{X}_k|\mathbf{Y}_{1:k}}} [f(\mathbf{x})] - \mathbb{E}_{\mathbf{y} \sim \pi_{\mathbf{X}_k|\mathbf{Y}_{1:k}}^{\mathcal{S}}} [f(\mathbf{y})] \right).$$

It is challenging to solve the optimization on the continuous function space  $\mathcal{C}(\Omega)$ . To make it efficient and feasible, we select an RKHS space  $\mathcal{H}$  defined on a compact metric space  $\Omega$  with reproducing kernel  $k(\cdot, \cdot)$ . When the kernel of  $\mathcal{H}$  is universal, the properties of the [Lemma 3.1](#) are held. Let  $\mathcal{F}$  be a unit ball in RKHS  $\mathcal{H}$ . Then  $\text{MMD}[p, q; \mathcal{F}] = 0$  if and only if  $p = q$ . The target of the optimization problem [\(3.7\)](#) can be rewritten as

$$(3.8) \quad \sup_{f \in \mathcal{F}} \left( \mathbb{E}_{\mathbf{x} \sim \pi_{\mathbf{X}_k|\mathbf{Y}_{1:k}}} [f(\mathbf{x})] - \mathbb{E}_{\mathbf{y} \sim \pi_{\mathbf{X}_k|\mathbf{Y}_{1:k}}^{\mathcal{S}}} [f(\mathbf{y})] \right).$$

The formula [\(3.8\)](#) is also called Maximum Mean Discrepancy(MMD). The MMD is a reasonable measure of the difference between two distributions. When MMD equals zero, two distributions are identical. With the reproducing property of RKHS, we do not need to compute the expectation of a specific function  $f$  directly. It suffices to compute [\(3.8\)](#) by [\(3.9\)](#) in the following lemma.

**Lemma 3.3.** *(Lemma 5 in [11]) Given  $\mathbf{x}$  and  $\mathbf{x}'$  independent variables with distribution  $p$ ,  $\mathbf{y}$  and  $\mathbf{y}'$  independent variables with distribution  $q$ . Assuming that the expectation of feature mapping  $\phi(\cdot)$  of RKHS  $\mathcal{H}$  exists. Then*

$$(3.9) \quad \text{MMD}^2[p, q; \mathcal{F}] = \mathbb{E}_{\mathbf{x}, \mathbf{x}' \sim p} [k(\mathbf{x}, \mathbf{x}')] - 2\mathbb{E}_{\mathbf{x} \sim p, \mathbf{y} \sim q} [k(\mathbf{x}, \mathbf{y})] + \mathbb{E}_{\mathbf{y}, \mathbf{y}' \sim q} [k(\mathbf{y}, \mathbf{y}')].$$

**3.2. Ensemble approximation of transport filter.** Motivated by the nudging method, we can construct the transport map  $\mathcal{T}_k$  by

$$(3.10) \quad \mathbf{X}_k = \mathcal{T}_k(\hat{\mathbf{X}}_k) = \hat{\mathbf{X}}_k + \mathbf{T}(\mathbf{Y}_k - \mathcal{H}(\hat{\mathbf{X}}_k)),$$

where  $\mathbf{T}(\cdot)$  can be a linear or nonlinear map. Transport map  $\mathcal{T}_k$  generates a transition probability that convert  $\pi_{\mathbf{X}_k|\mathbf{Y}_{1:k-1}}$  to  $q_{\mathbf{X}_k|\mathbf{Y}_{1:k}}^{\mathcal{T}_k}$ . Transport map  $\mathcal{T}_k$  is related to the observation  $\mathbf{y}_k$ . We select a parameterized function space  $\mathcal{G}_0$  and take map  $\mathbf{T}$  to be the function in  $\mathcal{G}_0$ . Then  $\mathcal{G}_0$  is transformed into space  $\mathcal{G}$  according to [\(3.10\)](#). We now aims to find an optimal transport map  $\mathcal{T}_k^* \in \mathcal{G}$  that minimizes the  $\text{MMD}^2$  loss



$$(3.11) \quad \mathcal{T}_k^* = \arg \min_{\mathcal{T}_k \in \mathcal{G}} \text{MMD}^2 \left[ \pi_{\mathbf{X}_k | \mathbf{Y}_{1:k}}^{\mathcal{T}_k}, \pi_{\mathbf{X}_k | \mathbf{Y}_{1:k}}; \mathcal{F} \right],$$

where  $\mathcal{F}$  is a unit ball of RKHS  $\mathcal{H}$ .

In the framework of ensemble-based filter method, we start from an ensemble of particles  $\{\mathbf{x}_{k-1}^{(i)}\}_{i=1}^N$  from the posterior density at time step  $k-1$ . Samples  $\{\hat{\mathbf{x}}_k^{(i)}\}_{i=1}^N$  of the prior density at time step  $k$  can be generated by the discrete dynamical model (2.1). Then the samples of prior density can be pushed forwards  $q_{\mathbf{X}_k | \mathbf{Y}_{1:k}}^{\mathcal{T}_k}$  by transport map  $\mathcal{T}_k$  in (3.10). In particle filtering, information on the true posterior density is implied in the weights of particles. We can express the reference posterior density as

$$(3.12) \quad \pi_{\mathbf{X}_k | \mathbf{Y}_{1:k}} \approx \sum_{i=1}^N w_i \delta_{\hat{\mathbf{x}}_k^{(i)}}(\mathbf{x}_k), w_i = \frac{\pi(\mathbf{y}_k | \hat{\mathbf{x}}_k^{(i)})}{\sum_{j=1}^N \pi(\mathbf{y}_k | \hat{\mathbf{x}}_k^{(j)})}.$$

The empirical estimation of  $\text{MMD}^2$  loss between approximated and true posterior density is given by the following formula [32],

$$(3.13) \quad \begin{aligned} \text{MMD}^2 = & \sum_{i,j=1}^m w_i w_j k(\hat{\mathbf{x}}_k^{(i)}, \hat{\mathbf{x}}_k^{(j)}) - 2 \sum_{i,j=1}^m w_i v_j k(\hat{\mathbf{x}}_k^{(i)}, \mathcal{T}_k(\hat{\mathbf{x}}_k^{(j)})) \\ & + \sum_{i,j=1}^n v_i v_j k(\mathcal{T}_k(\hat{\mathbf{x}}_k^{(i)}), \mathcal{T}_k(\hat{\mathbf{x}}_k^{(j)})), \end{aligned}$$

where  $\{v_i\}_{i=1}^N$  are weights of particles generated by transport map  $\mathcal{T}_k$  and  $v_i = 1/N$ .

**Remark 1.** *The selection of the kernel function in the ensemble transport filter is crucial in determining how well the ensemble transport filter approximates the posterior distribution. When we choose a universal kernel such as the Gaussian kernel  $k(\mathbf{x}, \mathbf{x}') = \exp(-\|\mathbf{x} - \mathbf{x}'\|/r^2)$ , ensemble transport filter will tend to approximate the posterior distribution as accurate as possible. When we choose a linear kernel function  $k(\mathbf{x}, \mathbf{x}') = \mathbf{x}^\top \mathbf{x}' + 1$ , it tends to obtain a better estimate of the mean of the posterior distribution and ignores higher order moment information. For further analysis, one can adaptively adjust the kernel functions based on the actual model, as discussed in [31].*

**Remark 2.** *A suitably chosen function space  $\mathcal{G}$  helps to improve the performance of the ensemble transport filter; one of the simplest choices is to take  $T$  to be a linear map as in EnKF, where all particles are uniformly complementary concerning the observation. This approach is computationally efficient. However, like EnKF, it performs poorly in strongly nonlinear cases. The function space can be learned by normalized flow, RBF mapping and particle flow [28]. In our numerical simulations, we learn it by fully connected neural networks.*

---

**Algorithm 3.1** Ensemble Transport map filter(EnTranF)
 

---

**Input:** Given ensemble  $\{\mathbf{x}_{k-1}^{(i)}\}_{i=1}^N$  at previous time step  $k-1$ , current observation  $\mathbf{y}_k^o$ , discrete dynamical model  $\mathcal{M}_k(\cdot)$ , observation operator  $\mathcal{H}_k(\cdot)$ , model uncertainty  $\pi(\boldsymbol{\eta}_k)$  and likelihood function  $\pi(\mathbf{y}_k | \mathbf{x}_k)$ ;

- 1: **for**  $i = 1, \dots, N$  **do**
  - 2:      $\hat{\mathbf{x}}_k^{(i)} = \mathcal{M}_k(\mathbf{x}_{k-1}^{(i)}) + \boldsymbol{\eta}_k^{(i)}$ ;
  - 3: **end for** ▷ Forecast Step
  - 4: Calculate particle weights  $w_i = \frac{\pi(\mathbf{y}_k^o | \hat{\mathbf{x}}_k^{(i)})}{\sum_{j=1}^N \pi(\mathbf{y}_k^o | \hat{\mathbf{x}}_k^{(j)})}$ ;
  - 5: Initialize transport map  $\mathcal{T}_k$  defined as (3.10);
  - 6: **repeat**
  - 7:     **for**  $i = 1, \dots, N$  **do**
  - 8:          $\mathbf{x}_k^{(i)} = \mathcal{T}_k(\hat{\mathbf{x}}_k^{(i)})$ ; ▷ Alternative Analysis Step
  - 9:          $v_i = 1/N$ ;
  - 10:     **end for**
  - 11:     Calculate MMD<sup>2</sup> loss by (3.13);
  - 12:     Update transport map  $\mathcal{T}_k$  using gradient descent.
  - 13: **until** Stopping criterion met
- Output:** Approximated posterior ensemble  $\{\mathbf{x}_k^{(i)}\}_{i=1}^N$ ;
- 

**3.3. Variance penalty for MMD loss.** Given the nonlinear nature of the optimization problem, we may learn a local optimal transport map and vanilla MMD loss is less efficient in high dimensional problems. To make the transport map better approximate the posterior distribution, we introduce a variance penalty term. It prioritizes minimizing the discrepancy between the expectations of highly informative statistics for the approximated and reference posteriors. Since  $\mathcal{F}$  is a unit ball of RKHS, the symmetry implies that

$$\left[ \sup_{f \in \mathcal{F}} (\mathbb{E}_{\mathbf{x} \sim p}[f(\mathbf{x})] - \mathbb{E}_{\mathbf{y} \sim q}[f(\mathbf{y})]) \right]^2 = \sup_{f \in \mathcal{F}} (\mathbb{E}_{\mathbf{x} \sim p}[f(\mathbf{x})] - \mathbb{E}_{\mathbf{y} \sim q}[f(\mathbf{y})])^2.$$

The MMD loss with variance penalty is defined by

$$(3.14) \quad \text{Loss} = \sup_{f \in \mathcal{F}} \left\{ (\mathbb{E}_{\mathbf{x} \sim p}[f(\mathbf{x})] - \mathbb{E}_{\mathbf{y} \sim q}[f(\mathbf{y})])^2 + \lambda (\text{Var}_{\mathbf{x} \sim p}[f(\mathbf{x})] + \text{Var}_{\mathbf{y} \sim q}[f(\mathbf{y})]) \right\},$$

where  $0 \leq \lambda \leq 1$  is a regularization parameter. By a direct calculation, we can rewrite (3.14) as

$$(3.15) \quad \text{Loss} = \sup_{f \in \mathcal{F}} \left\{ (1 - \lambda) (\mathbb{E}_{\mathbf{x} \sim p}[f(\mathbf{x})] - \mathbb{E}_{\mathbf{y} \sim q}[f(\mathbf{y})])^2 + \lambda \mathbb{E}_{\substack{\mathbf{x} \sim p, \\ \mathbf{y} \sim q}} [f(\mathbf{x}) - f(\mathbf{y})]^2 \right\}.$$

In (3.15), training loss is split into two terms. The first term  $(\mathbb{E}_{\mathbf{x} \sim p}[f(\mathbf{x})] - \mathbb{E}_{\mathbf{y} \sim q}[f(\mathbf{y})])^2$  constrain the mean of two densities to be close, while the second term  $\mathbb{E}[f(\mathbf{x}) - f(\mathbf{y})]^2$

forces the distance of two related samples to be close. Two component terms of training loss are positive, and an upper bound estimate of (3.14) can be given by optimizing two component terms separately. The first term remains to be MMD, which can be interpreted as (3.9). Since  $f \in \mathcal{F}$  and  $\|f\|_{\mathcal{H}} \leq 1$ , then

$$\begin{aligned} \sup_{f \in \mathcal{F}} \mathbb{E} [f(\mathbf{x}) - f(\mathbf{y})]^2 &= \sup_{f \in \mathcal{F}} \mathbb{E} [\langle \phi_{\mathbf{x}} - \phi_{\mathbf{y}}, f \rangle_{\mathcal{H}}^2] \\ &= \sup_{f \in \mathcal{F}} \mathbb{E} \left[ \|\phi_{\mathbf{x}} - \phi_{\mathbf{y}}\|_{\mathcal{H}}^2 \left\langle \frac{\phi_{\mathbf{x}} - \phi_{\mathbf{y}}}{\|\phi_{\mathbf{x}} - \phi_{\mathbf{y}}\|_{\mathcal{H}}}, f \right\rangle_{\mathcal{H}}^2 \right], \end{aligned}$$

where  $\phi_{\mathbf{x}} = k(\mathbf{x}, \cdot)$  and  $\phi_{\mathbf{y}} = k(\mathbf{y}, \cdot)$ . With Cauchy inequality, it gives

$$\left\langle \frac{\phi_{\mathbf{x}} - \phi_{\mathbf{y}}}{\|\phi_{\mathbf{x}} - \phi_{\mathbf{y}}\|_{\mathcal{H}}}, f \right\rangle_{\mathcal{H}} \leq \frac{\|\phi_{\mathbf{x}} - \phi_{\mathbf{y}}\|_{\mathcal{H}}}{\|\phi_{\mathbf{x}} - \phi_{\mathbf{y}}\|_{\mathcal{H}}} \|f\|_{\mathcal{H}} \leq 1.$$

When  $f = \frac{\phi_{\mathbf{x}} - \phi_{\mathbf{y}}}{\|\phi_{\mathbf{x}} - \phi_{\mathbf{y}}\|_{\mathcal{H}}} \in \mathcal{F}$ , the equality holds. Thus

$$\sup_{f \in \mathcal{F}} \mathbb{E} [f(\mathbf{x}) - f(\mathbf{y})]^2 = \mathbb{E} [\|\phi_{\mathbf{x}} - \phi_{\mathbf{y}}\|_{\mathcal{H}}^2].$$

Then the second term of (3.15) can be rewritten as

$$(3.16) \quad \sup_{f \in \mathcal{F}} \mathbb{E} [f(\mathbf{x}) - f(\mathbf{y})]^2 = \mathbb{E}_{\mathbf{x} \sim p} [k(\mathbf{x}, \mathbf{x})] - 2\mathbb{E}_{\mathbf{x} \sim p, \mathbf{y} \sim q} [k(\mathbf{x}, \mathbf{y})] + \mathbb{E}_{\mathbf{y} \sim p} [k(\mathbf{y}, \mathbf{y})].$$

Similar to (3.13), we can estimate (3.16) with ensemble particles, i.e.,

$$\begin{aligned} \sup_{f \in \mathcal{F}} \mathbb{E} [f(\mathbf{x}) - f(\mathbf{y})]^2 &= \sum_{i=1}^m w_i k(\hat{\mathbf{x}}_k^{(i)}, \hat{\mathbf{x}}_k^{(i)}) - 2 \sum_{i,j=1}^m w_i v_j k(\hat{\mathbf{x}}_k^{(i)}, \mathcal{T}_k(\hat{\mathbf{x}}_k^{(j)})) \\ &\quad + \sum_i^n v_i k(\mathcal{T}_k(\hat{\mathbf{x}}_k^{(i)}), \mathcal{T}_k(\hat{\mathbf{x}}_k^{(i)})), \end{aligned}$$

where  $\{v_i = 1/N\}_{i=1}^N$  are weights of particles generated by transport map  $\mathcal{T}_k$  and  $\{w_i\}_{i=1}^N$  are weights of particle filter defined in (3.12).

If we restrict the kernel function to be the linear kernel and the search space of the transport map to be linear, we can obtain an analytical form of the transport map filter.

**Theorem 3.4.** *Given the RKHS kernel  $k(\mathbf{x}, \mathbf{x}') = \mathbf{x}^\top \mathbf{x}' + 1$  and regularization parameter  $\lambda = 1$ . Moreover, we assume (3.10) to be a linear transport, i.e.,*

$$(3.17) \quad \mathbf{X}_k^{\mathcal{T}_k} = \hat{\mathbf{X}}_k + \mathbf{T}(\mathbf{y}_k + \boldsymbol{\varepsilon}_k - \mathcal{H}(\hat{\mathbf{X}}_k)),$$

where  $\mathbf{T} \in \mathbb{R}^{m \times n}$ ,  $\mathbf{y}_k = \mathcal{H}_k(\mathbf{x}_k)$  and  $\boldsymbol{\varepsilon}_k$  is independent with  $\hat{\mathbf{X}}_k$ . Denote

$$\begin{aligned} \bar{\mathbf{X}}_k &= \hat{\mathbf{X}}_k - \mathbb{E}[\mathbf{X}_k], \\ \bar{\mathbf{Y}}_k &= \mathcal{H}(\hat{\mathbf{X}}_k) - \mathbf{y}_k. \end{aligned}$$

Then the optimization problem (3.11) has the global optimal solution

$$(3.18) \quad \mathbf{T} = \mathbb{E} \left[ \bar{\mathbf{X}}_k \bar{\mathbf{Y}}_k^\top \right] \left\{ \mathbb{E} \left[ \bar{\mathbf{Y}}_k \bar{\mathbf{Y}}_k^\top \right] + \mathbb{E}[\boldsymbol{\varepsilon}_k \boldsymbol{\varepsilon}_k^\top] \right\}^{-1}.$$

*Proof.* By plugging (3.17) into (3.11), the MMD loss can be rewritten as

$$\begin{aligned} \text{MMD}[p, q; \mathcal{F}] &= \mathbb{E}[(\mathbf{y}_k + \boldsymbol{\varepsilon}_k - \mathcal{H}(\hat{\mathbf{X}}_k))^\top \mathbf{T}^\top \mathbf{T} (\mathbf{y}_k + \boldsymbol{\varepsilon}_k - \mathcal{H}(\hat{\mathbf{X}}_k))] \\ &\quad + 2\mathbb{E}[\hat{\mathbf{X}}_k^\top \mathbf{T} (\mathbf{y}_k + \boldsymbol{\varepsilon}_k - \mathcal{H}(\hat{\mathbf{X}}_k))] \\ &\quad - 2\mathbb{E}[\mathbf{X}_k^\top \mathbf{T} (\mathbf{y}_k + \boldsymbol{\varepsilon}_k - \mathcal{H}(\hat{\mathbf{X}}_k))] \\ &\quad + C. \end{aligned}$$

We take  $\frac{\partial \text{MMD}[p, q; \mathcal{F}]}{\partial \mathbf{T}} = 0$ . According to the property of matrix derivatives

$$\frac{\partial \mathbf{a}^\top \mathbf{x} \mathbf{b}}{\partial \mathbf{x}} = \mathbf{a} \mathbf{b}^\top, \quad \frac{\partial \mathbf{b}^\top \mathbf{x}^\top \mathbf{x} \mathbf{c}}{\partial \mathbf{x}} = \mathbf{x} (\mathbf{b} \mathbf{c}^\top + \mathbf{c} \mathbf{b}^\top),$$

we have

$$\begin{aligned} \mathbf{T} \mathbb{E}[(\mathbf{y}_k + \boldsymbol{\varepsilon}_k - \mathcal{H}(\hat{\mathbf{X}}_k))(\mathbf{y}_k + \boldsymbol{\varepsilon}_k - \mathcal{H}(\hat{\mathbf{X}}_k))^\top] &= \mathbb{E}[\hat{\mathbf{X}}_k (\mathbf{y}_k + \boldsymbol{\varepsilon}_k - \mathcal{H}(\hat{\mathbf{X}}_k))^\top] \\ &\quad - \mathbb{E}[\mathbf{X}_k (\mathbf{y}_k + \boldsymbol{\varepsilon}_k - \mathcal{H}(\hat{\mathbf{X}}_k))^\top]. \end{aligned}$$

Because  $\pi_{\mathbf{X}_k | \mathbf{Y}_{1:k}}^{\mathcal{T}_k}$  and  $\pi_{\mathbf{X}_k | \mathbf{Y}_{1:k}}$  in (3.11) are two different distributions, the corresponding random variables  $\mathbf{X}_k^{\mathcal{T}_k}$  and  $\mathbf{X}_k$  are set to be independent. Thus

$$\begin{aligned} \mathbf{T} \left\{ \mathbb{E}[(\mathbf{y}_k - \mathcal{H}(\hat{\mathbf{X}}_k))(\mathbf{y}_k - \mathcal{H}(\hat{\mathbf{X}}_k))^\top] + \mathbb{E}[\boldsymbol{\varepsilon}_k \boldsymbol{\varepsilon}_k^\top] \right\} &= \mathbb{E}[\hat{\mathbf{X}}_k (\mathbf{y}_k - \mathcal{H}(\hat{\mathbf{X}}_k))^\top] \\ &\quad - \mathbb{E}[\mathbf{X}_k] \mathbb{E}[\mathbf{y}_k - \mathcal{H}(\hat{\mathbf{X}}_k)]^\top. \end{aligned}$$

Let  $\bar{\mathbf{X}}_k := \hat{\mathbf{X}}_k - \mathbb{E}[\mathbf{X}_k]$ ,  $\bar{\mathbf{Y}}_k = \mathcal{H}(\hat{\mathbf{X}}_k) - \mathbf{y}_k$ . Then we have

$$\mathbf{T} = \mathbb{E} \left[ \bar{\mathbf{X}}_k \bar{\mathbf{Y}}_k^\top \right] \left\{ \mathbb{E} \left[ \bar{\mathbf{Y}}_k \bar{\mathbf{Y}}_k^\top \right] + \mathbb{E}[\boldsymbol{\varepsilon}_k \boldsymbol{\varepsilon}_k^\top] \right\}^{-1}.$$

Proof is completed. ■

Since exact states  $\mathbf{x}_k$  and observation  $\mathcal{H}_k(\mathbf{x}_k)$  are not available, we approximate  $\mathbf{Y}_k$  by  $\mathbf{y}_k^o + \boldsymbol{\varepsilon}_k$ . By (3.12), the expectation of posterior  $\mathbb{E}[\mathbf{X}_k] \approx \sum_{i=1}^N w_i \hat{\mathbf{x}}_k^{(i)}$ . The ensemble

approximation of (3.18) are computed by

$$(3.19) \quad \mathbb{E} \left[ \bar{\mathbf{X}}_k \bar{\mathbf{Y}}_k^\top \right] \approx \frac{1}{N-1} \sum_{i=1}^N \left( \hat{\mathbf{x}}_k^{(i)} - \mathbb{E}[\mathbf{X}_k] \right) \left( \mathcal{H}(\hat{\mathbf{x}}_k^{(i)}) - \mathbf{y}_k^o \right)^\top,$$

$$(3.20) \quad \mathbb{E} \left[ \bar{\mathbf{Y}}_k \bar{\mathbf{Y}}_k^\top \right] \approx \frac{1}{N-1} \sum_{i=1}^N \left( \mathcal{H}(\hat{\mathbf{x}}_k^{(i)}) - \mathbf{y}_k^o \right) \left( \mathcal{H}(\hat{\mathbf{x}}_k^{(i)}) - \mathbf{y}_k^o \right)^\top,$$

$$(3.21) \quad \mathbb{E}[\boldsymbol{\varepsilon}_k \boldsymbol{\varepsilon}_k^\top] \approx \frac{1}{N-1} \sum_{i=1}^N \left( \boldsymbol{\varepsilon}_k^{(i)} \boldsymbol{\varepsilon}_k^{(i)} \right)^\top,$$

where  $\{\boldsymbol{\varepsilon}_k^{(i)}\}_{i=1}^N$  are drawn from observation noise.

---

**Algorithm 3.2** EnTranF with variance penalty(EnTranFp) on [Theorem 3.4](#)

---

**Input:** Given ensemble  $\{\mathbf{x}_{k-1}^{(i)}\}_{i=1}^N$  at previous time step  $k-1$ , current observation  $\mathbf{y}_k^o$ , discrete dynamical model  $\mathcal{M}_k(\cdot)$ , observation operator  $\mathcal{H}_k(\cdot)$ , model uncertainty  $\pi(\boldsymbol{\eta}_k)$  and likelihood function  $\pi(\mathbf{y}_k | \mathbf{x}_k)$ ;

1: **for**  $i = 1, \dots, N$  **do**

2:      $\hat{\mathbf{x}}_k^{(i)} = \mathcal{M}_k(\mathbf{x}_{k-1}^{(i)}) + \boldsymbol{\eta}_k^{(i)}$ ;

3: **end for**

▷ Forecast Step

4: Calculate particle weights  $w_i = \frac{\pi(\mathbf{y}_k^o | \hat{\mathbf{x}}_k^{(i)})}{\sum_{j=1}^N \pi(\mathbf{y}_k^o | \hat{\mathbf{x}}_k^{(j)})}$ ;

5: Calculate  $\mathbf{T}$  in (3.17) with ensemble approximation (3.19)-(3.21);

6: **for**  $i = 1, \dots, N$  **do**

7:      $\mathbf{x}_k^{(i)} = \hat{\mathbf{x}}_k^{(i)} + \mathbf{T}(\mathbf{y}_k^o + \boldsymbol{\varepsilon}_k - \mathcal{H}(\hat{\mathbf{x}}_k^{(i)}))$ ;

▷ Alternative Analysis Step

8: **end for**

**Output:** Approximated posterior ensemble  $\{\mathbf{x}_k^{(i)}\}_{i=1}^N$ ;

---

**Remark 3.** Equation (3.18) shows that the ensemble transport filter with a variance penalty MMD loss has a similar form compared to the EnKF with a linear assumption and linear kernel. Denote

$$\tilde{\mathbf{X}}_k = \hat{\mathbf{X}}_{k+1} - \mathbb{E}[\hat{\mathbf{X}}_{k+1}], \quad \tilde{\mathbf{Y}}_k = \mathcal{H}(\hat{\mathbf{X}}_{k+1}) - \mathbb{E} \left[ \mathcal{H}(\hat{\mathbf{X}}_{k+1}) \right].$$

the Kalman gain of EnKF can be rewritten as

$$(3.22) \quad \mathbf{K} = \mathbb{E} \left[ \tilde{\mathbf{X}}_k \tilde{\mathbf{Y}}_k^\top \right] \left\{ \mathbb{E} \left[ \tilde{\mathbf{Y}}_k \tilde{\mathbf{Y}}_k^\top \right] + \mathbb{E}[\boldsymbol{\varepsilon}_{k+1} \boldsymbol{\varepsilon}_{k+1}^\top] \right\}^{-1}.$$

The main difference between EnTranF and EnKF is that the means of  $\hat{\mathbf{X}}_{k+1}$  and  $\mathcal{H}(\hat{\mathbf{X}}_{k+1})$  are approximated by  $\mathbb{E}[\mathbf{X}_{k+1}]$  and  $\mathbf{y}_k$ , respectively, in EnTranF. This drives the prior particles towards the posterior mean as dictated by transport map (3.17).

**Remark 4.** When the RKHS kernel takes  $k(\mathbf{x}, \mathbf{x}') = \mathbf{x}^\top \mathbf{x}' + 1$  and take regularization parameter to be  $\lambda = 0$ , we follow the proof of [Theorem 3.4](#) and get

$$(3.23) \quad \mathbf{T} = \mathbb{E}[\bar{\mathbf{X}}_k] \mathbb{E}[\bar{\mathbf{Y}}_k]^\top \left\{ \mathbb{E}[\bar{\mathbf{Y}}_k] \mathbb{E}[\bar{\mathbf{Y}}_k]^\top \right\}^{-1}.$$

Formally, [\(3.18\)](#) provides a complete slope in the statistical least squares sense, while [\(3.23\)](#) gives the geometric slope from the prior mean to the posterior mean. However, when the number of particles is small, [\(3.23\)](#) may be numerically unstable.

**4. Numerical Results.** In this section, we will use a few numerical examples to illustrate the advantage of the EnTranF over ensemble Kalman filtering in the data assimilation. A static inverse problem is implemented to show the capability of EnTranF in approximating posterior distributions in [subsection 4.1](#). In [subsection 4.2](#), we discuss the performance of EnTranF in nonlinear system by tracking Double-Well system. For strongly nonlinear cases, we consider the filtering problem of the Lorenz63 system with partial observations in [subsection 4.3](#). Finally, the performance of EnTranF for tracking high-dimensional systems is demonstrated in [subsection 4.4](#).

We use component average Root-Mean-Squared Error (RMSE) to evaluate the performance of the assimilation method, which is defined by

$$\text{RMSE}_k := \|\bar{\mathbf{x}}_k - \mathbf{x}_k^*\|_2 / \sqrt{n}$$

at any assimilation step  $k$ . Here  $\bar{\mathbf{x}}_k \in \mathbb{R}^n$  is the (ensemble) mean state generated by the data assimilation method, and  $\mathbf{x}_k^* \in \mathbb{R}^n$  is the reference state. Considering all assimilation windows throughout the filtering process, we compute the time-averaged RMSE. Meanwhile, to eliminate the influence of randomness, we define the final performance metric RMSE as its expectation, i.e.,

$$(4.1) \quad \text{RMSE} = \mathbb{E} \left[ \frac{1}{T} \sum_{k=1}^T \|\bar{\mathbf{x}}_k - \mathbf{x}_k^*\|_2 / \sqrt{n} \right].$$

Moreover, Ensemble Spread(ENS) is used to measure the concentration of the ensemble samples, which is computed by  $\text{ENS}_k = [\text{tr}(\mathbf{C}_k^a)/n]^{1/2}$ , where  $\mathbf{C}_k^a$  is the analysis ensemble covariance matrix at time step  $k$ . Similarly, a time average is used to monitor the ENS over the whole assimilation process.

$$(4.2) \quad \text{ENS} = \mathbb{E} \left[ \frac{1}{T} \sum_{k=1}^T [\text{tr}(\mathbf{C}_k^a)/n]^{1/2} \right].$$

We will use Coverage Probability (CP) to fully assess RMSE and Ensemble Spread. CP refers to the probability, with which a confidence interval of the filtered state encompasses the reference. A higher CP indicates better consistency between the filtered and reference states. Here, we define CP by

$$(4.3) \quad \text{CP} = \mathbb{E} \left[ \frac{1}{n} \sum_{i=1}^n \left( \frac{1}{T} \sum_{k=1}^T \mathbb{I}_{|\bar{\mathbf{x}}_{k,i} - \mathbf{x}_{k,i}^*| / \sqrt{\mathbf{C}_{k,(i,i)}^a} \leq t_\alpha} \right) \right],$$

where  $\mathbb{I}$  is indicator function and  $t_\alpha$  is  $\alpha$  quantiles of standard normal distribution. We computed the expectation in (4.1)-(4.3) using 20 repeated tests.

**4.1. Static inverse problem.** In this subsection, we consider two static inverse problems to examine the validity of the transport map from the prior to the posterior distribution based on the MMD loss function. We will compare the EnTranF with the EnKF and examine how well it approximates the true posterior distribution.

Start with a one-dimensional example, and suppose  $X$  is a random variable with Gaussian prior and Gaussian observation noise. The nonlinear observation operator is considered as  $\mathcal{H}(x) = 2x^3 + x$ . The task is to estimate the Bayesian posterior of the  $X$  given values of observations  $y^o$ . In EnTranF and EnKF, particles are generated to approximate the posterior distribution. Then, a kernel density estimate method is used to evaluate the density function of ensembles. For reference, based on Bayes' rule

$$\pi_{posterior}(x | y) \propto \pi_{prior}(x) \times \pi_{likelihood}(y | x),$$

The exact posterior density can be calculated using the numerical integral method.

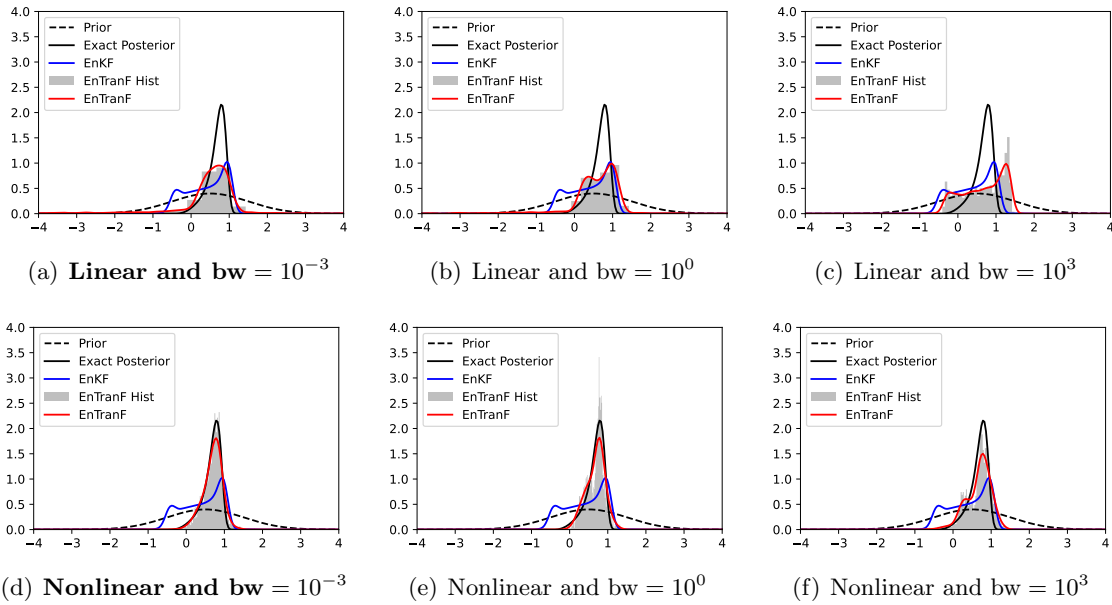


**Figure 3.** Posterior approximation of EnTranF with Linear transport map (Panel (a)-(c)) and Nonlinear transport map (Panel (d)-(f)) when taking different bandwidths of MMD loss. The example considered the influence of bandwidth at different scales ( $10^{-3}$ ,  $10^0$  and  $10^3$ ) on EnTranF.

We select Gaussian kernel for MMD loss with three different bandwidth values  $10^{-3}$ ,  $10^0$ , and  $10^3$ . Linear and Nonlinear transport maps are used to approximate posterior in EnTranF, and the results are shown in Figure 3. Larger bandwidth  $bw = 10^3$  leads to more accurate estimates of the mean compared to EnKF, but it fails to capture the morphology of the posterior distribution. When a smaller bandwidth ( $bw = 10^0$  and

bw =  $10^{-3}$ ) is given, estimation of the posterior distribution is more concentrated in the high-probability region of the true posterior distribution. EnTranF becomes more sensitive to the local details of the posterior distribution when a smaller bandwidth is chosen.

The nonlinear observation operator leads to the non-Gaussian of the posterior distribution. Both EnKF and EnTranF with linear transport maps fail to approximate the posterior distribution. As shown in [Figure 3](#), EnTranF achieves a significant improvement in approximating posterior distribution with a nonlinear transport map. This could be caused by the substantially different sensitivity of observations to the model state for each ensemble particle in the nonlinear assimilation problem. A linear form of transport map may not well approximate a non-Gaussian posterior.

At the same time, we will examine the performance of EnTranF, which optimizes the MMD with a variance penalty in approximating the posterior distribution. The penalized EnTranF is compared to the case without a penalty term on a two-dimensional state space  $\mathbf{x} = [\mathbf{x}_1, \mathbf{x}_2]$ . We still assume Gaussian prior and the nonlinear observation function  $\mathcal{H}(\mathbf{x}) = \mathbf{x}_1^3 + \mathbf{x}_2$ .

From [Figure 4](#), EnTranF and EnTranFp achieve accurate estimate of the posterior distribution, while EnKF has a significant bias. The particles of EnTranFp are more concentrated than EnTranF, and the variance penalty effectively improves the approximation of the posterior distribution in high-probability regions. [Table 1](#) lists the posterior mean and maximum a posteriori estimation(MAP) for different filtering methods. EnTranF performs the best on the posterior mean. EnTranFp performs slightly worse than EnTranF on the posterior mean, but they give a better MAP.

**Table 1**

*Estimation posterior mean and maximum a posteriori of the 2d static inverse problem*

		Reference	EnKF	EnTranF	EnTranFp
Mean	$x_0$	0.2434	0.2911	<b>0.2504</b>	0.2921
	$x_1$	0.5816	0.4478	<b>0.5551</b>	0.5565
MAP	$x_0$	0.5930	0.7940	0.3719	<b>0.4925</b>
	$x_1$	0.5729	0.5729	0.6533	<b>0.5528</b>

**4.2. Double-Well potential.** Double-well potential is a common form of potential energy in physics and chemistry. It is typically used to describe the movement of molecules or particles in bistable systems, often characterized by two local energy minima that allow particles to oscillate between these two points under random perturbations. This potential form is essential in describing various physical and chemical phenomena, such as conformational transitions within molecules and spin flips in magnetic materials. This subsection mainly demonstrates the performance of the EnTranF method for nonlinear filtering problem in tracking the Double-Well potential system. The dynamical



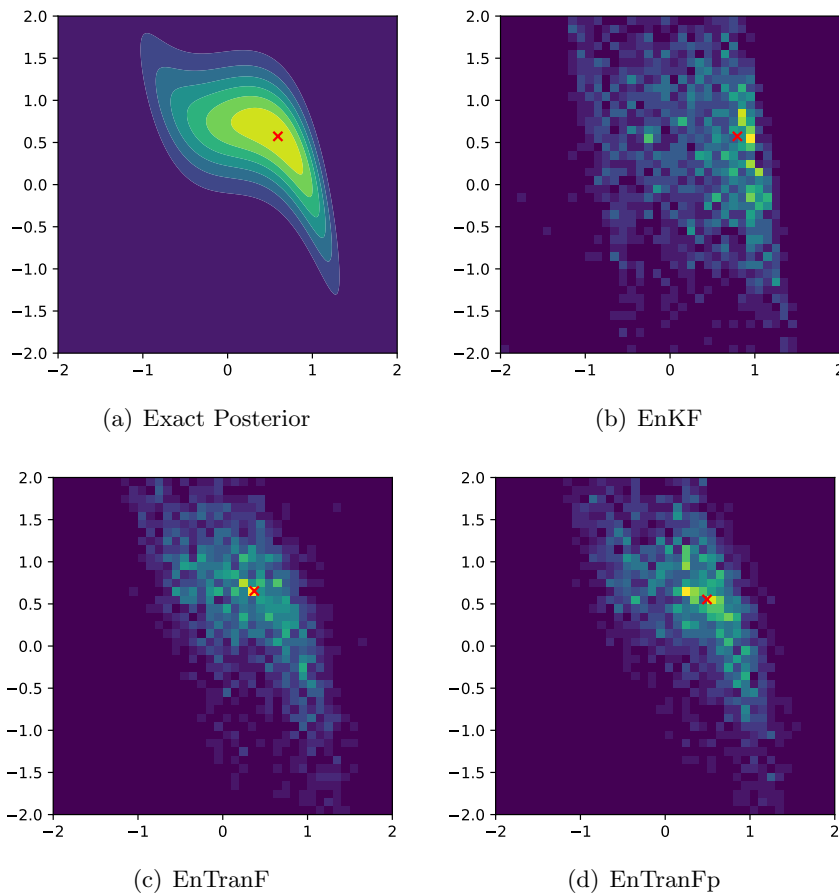


**Figure 4.** 2-d Histogram of ensemble particles generated by EnKF, EnTranF and EnTranFp. Red "x" represents the MAP estimation of the corresponding method.

model and observation operator are given by

$$(4.4) \quad dx = (x - x^3)dt + \gamma dW_t,$$

$$(4.5) \quad z = 0.1x^2 + \sin(x) + \epsilon,$$

where  $W_t$  is a standard brownian motion and  $\epsilon$  is Gaussian noise with  $\epsilon \sim \mathcal{N}(0, \sigma^2)$ . We take  $\gamma = 0.8$  and  $\sigma = 0.5$ . In this example, the fourth-order Runge-Kutta method is used to simulate the ODE system (4.4) with a constant discrete step size  $\Delta t = 0.01$ . Results of EnTranF with linear and nonlinear transport map are demonstrated.

For simplicity of notation, we use the following abbreviation to denote the ensemble transport filter:

- EnTranF(L-L): the ensemble transport filter with linear transport map and linear kernel function;
- EnTranF(L-G): the ensemble transport filter with linear transport map and Gaussian kernel function;

- EnTranF(N-L): the ensemble transport filter with nonlinear transport map and linear kernel function;
- EnTranF(N-G): the ensemble transport filter with nonlinear transport map and Gaussian kernel function;

Figure 5 compares the average RMSE between EnTranF and EnKF with different observation intervals and ensemble sizes.

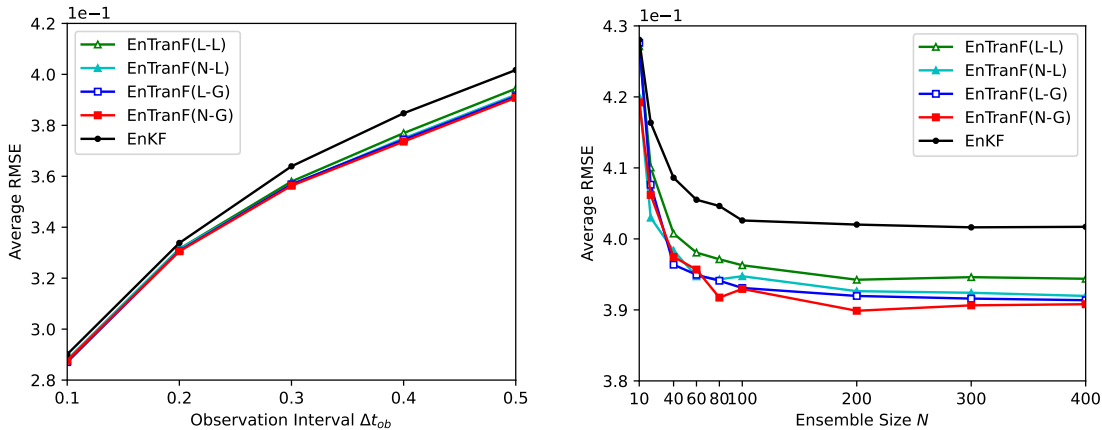
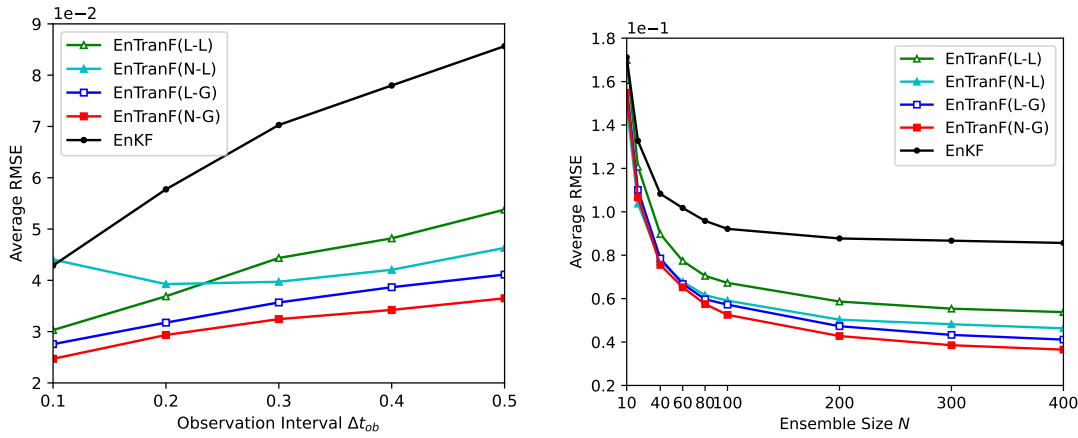


Figure 5. Average RMSE of Double-Well system for ensemble size  $N = 400$  as a function of observation interval (Left), and for observation interval  $\Delta t_{ob} = 0.5$  as a function of ensemble size (Right).

The left panel of Figure 5 indicates that EnTranF exhibits significant improvement on average RMSE compared to EnKF at larger observation intervals  $\Delta_{ob} > 0.2$  while performing similarly at smaller observation intervals. The nonlinearity of the filtering problem increases as the observation interval increases, leading to a larger difference in RMSE between EnKF and EnTranF. EnTranF(N-G) demonstrates the best performance. However, compared to EnTranF(N-L) and EnTranF(L-G), the difference on average RMSE is small. The right panel of Figure 5 shows that EnTranF achieves a smaller average RMSE compared to EnKF as the increase of ensemble size. Nonlinear transport maps exhibit better performance on average RMSE than linear transport maps. However, the difference is insignificant when taking the Gaussian kernel function. The EnTranF based on Gaussian kernel function keeps sufficient posterior information in filtering.

Since the DoubleWell potential represents a low-dimensional system, employing a particle filter with 10,000 particles as a benchmark posterior allows us to illustrate the approximate performance of EnTranF on the true posterior filtering distribution. To this end, we assess the tracking performance of the EnTranF using metrics identical to those employed to evaluate the estimation of the true state. Results are shown in Figure 6.

When measuring the performance of EnTranF in tracking the posterior mean, it exhibits a significant improvement on average RMSE compared to EnKF. From the left



**Figure 6.** Take posterior mean of PF with 10,000 particles as reference, Average RMSE of Double-Well system for ensemble size  $N = 400$  as a function of observation interval (left), and for observation interval  $\Delta t_{ob} = 0.5$  as a function of ensemble size (right).

panel of Figure 6, it can be observed that EnTranF shows an average improvement of 38.16% compared to EnKF across various observation intervals. At the same time, as the observation interval increases, the rate of increase in RMSE for EnTranF is lower than that for EnKF. This implies that EnTranF has better robustness as the nonlinearity increases. EnTranF(N-L) exhibits poor performance when the observation interval is 0.1, which may stem from inadequate optimization of the nonlinear transport map and getting trapped in local minima. As shown in the right panel of Figure 6, EnTranF gradually approaches reference solution as the number of particles increases. However, the average RMSE of EnKF do not decrease when the ensemble size becomes larger than 200.

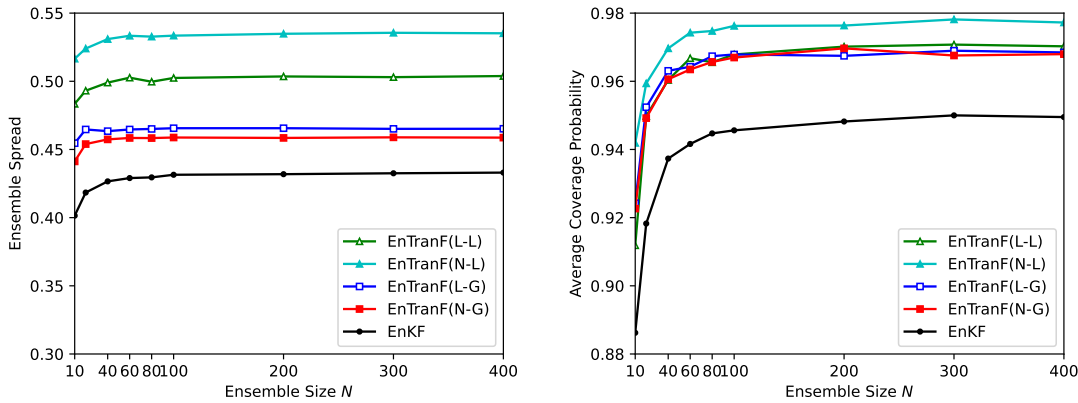


**Figure 7.** Left Panel: Spread of Double-Well system for observation interval  $\Delta t_{ob} = 0.5$  as a function of ensemble size. Right panel: Average coverage probability of Double-Well system for observation interval  $\Delta t_{ob} = 0.5$  as a function of ensemble size

While EnTranF demonstrates excellent performance in state estimation, its performance on ensemble spread is poor, leading to inadequate particle dispersion in ensemble filtering methods (see Figure 7). EnTranF also suffers from numerical overflow when the number of particles is low. After incorporating a variance penalty term, EnTranF can effectively address these issues. Figure 8 shows the RMSE and Spread of EnTranFp for different observation intervals and ensemble sizes.

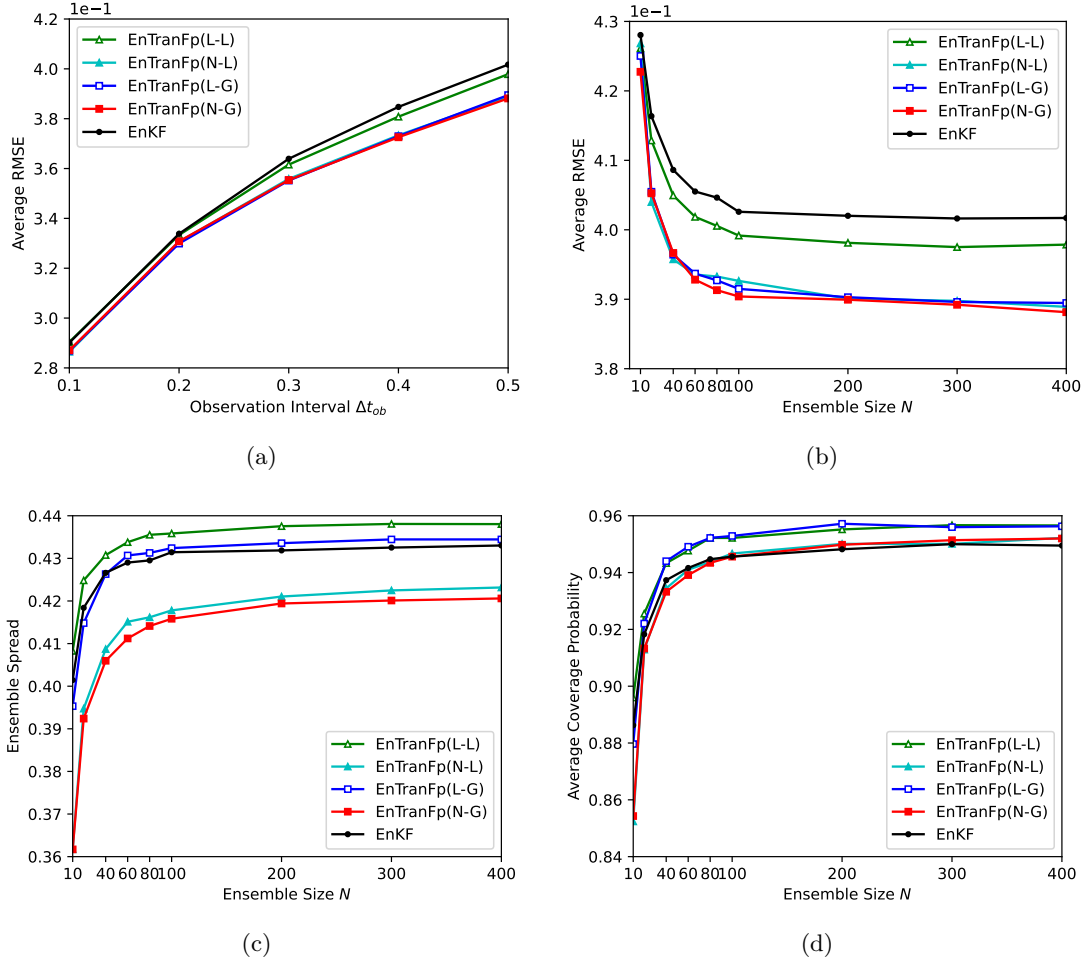


**Figure 8.** *EnTranF with variance penalty: Average RMSE of Double-Well system for ensemble size  $N = 400$  as a function of observation interval (Panel (a)), and for observation interval  $\Delta t_{ob} = 0.5$  as a function of ensemble size (Panel (b)). Spread of Double-Well system for observation interval  $\Delta t_{ob} = 0.5$  as a function of ensemble size (Panel (c)). Average coverage probability of Double-Well system for observation interval  $\Delta t_{ob} = 0.5$  as a function of ensemble size (Panel (d))*

From Figure 5 and Figure 8 (a)-(b), the average RMSE of EnTranFp remains consistent across different observation intervals and ensemble sizes. The EnTranFp maintains the accuracy of EnTranF in state estimation. EnTranFp(N-L), EnTranFp(L-G) and EnTranFp(N-G) show a small improvement compare to EnTranF in average RMSE. In

panel (c) and (d) of [Figure 8](#), EnTranFp with linear transport map exhibits a similar ensemble spread to EnKF. But it has a significantly higher probability of covering the true state. EnTranFp with a nonlinear transport map reduces the Spread while simultaneously increasing the probability of covering the true state. Compare with the results of EnTranF in [Figure 7](#), the EnTranFp enhances the robustness of the EnTranF and leads to a better approximation of the posterior.

**4.3. Lorenz’63 System.** Lorenz63 is a classic, chaotic system model proposed by American meteorologist Edward Lorenz in 1963. It describes the nonlinear dynamical behavior in atmospheric circulation. The Lorenz63 model is based on three partial differential equations and has three state variables:  $X_1$ ,  $X_2$ , and  $X_3$ . This model is known for its highly sensitive initial conditions and nonlinear coupling. It leads to the famous “butterfly effect” where a small perturbation of initial condition may result in long-term uncertainty and unpredictable outcomes. It can be expressed in the form of ODEs

$$(4.6) \quad \begin{aligned} \frac{dX_1}{dt} &= -\sigma X_1 + \sigma X_2 + \gamma_1 \frac{dB_1}{dt}, \\ \frac{dX_2}{dt} &= -X_1 X_3 + \rho X_1 - X_2 + \gamma_2 \frac{dB_2}{dt}, \\ \frac{dX_3}{dt} &= X_1 X_2 - \beta X_3 + \gamma_3 \frac{dB_3}{dt}, \end{aligned}$$

where  $B_1, B_2$  and  $B_3$  are standard Brownian motion. Here, the parameters are set to be  $\beta = 8/3, \rho = 28, \sigma = 10$ , which produces the well-known Lorenz attractor. The noise level of the different components is set to be the same  $\gamma_1 = \gamma_2 = \gamma_3 = 1.0$ . We simulate the ODEs (4.6) by using a fourth-order Runge-Kutta method with time stepsize  $\Delta t = 0.01$ . Here, we only take the observation operator to observe its first component. Partial observations greatly enhance the complexity and nonlinearity of the filtering problem. At the same time, we consider observations with Gaussian white noise.

At first, we assimilate the Lorenz’63 system with the default setup of the ensemble transport filter. [Figure 9](#) and [Figure 10](#) respectively show the average RMSE and Spread versus a range of observation interval and ensemble size.

As shown in the left panel of [Figure 9](#), we demonstrate the average RMSE of EnTranF as a function of observation interval with a fixed ensemble size. EnTranF(L-L) and EnTranF(N-L) experienced a collapse in the Lorenz’63 system, rendering it unable to produce meaningful state estimates. This is because the linear kernel function results in significant information loss at each assimilation window, making the method ineffective as sequential filtering progresses. EnTranF with a Gaussian kernel still performs well. EnTranF(L-G) and EnTranF(N-G) show a slight performance improvement compared to EnKF when the observation interval is relatively short. However, for sufficiently large observation intervals, they present an increasing improvement on RMSE compared to EnKF as the observation interval increases. EnTranF(N-G) and

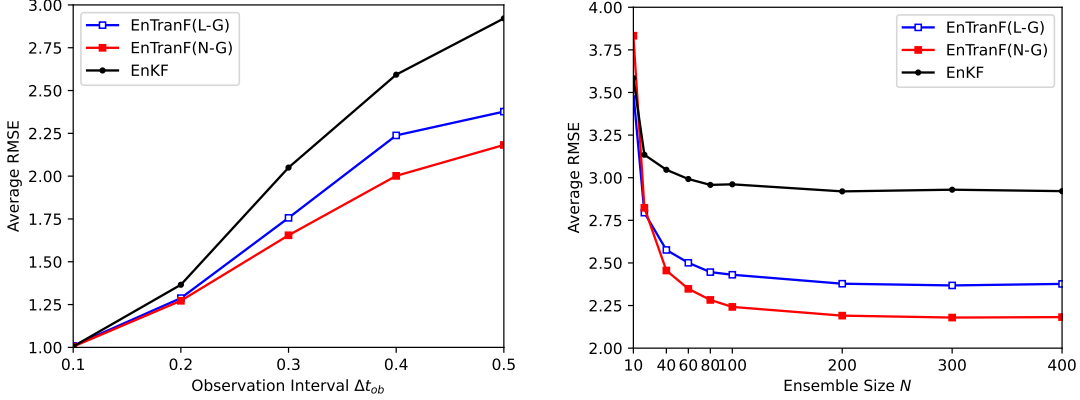


**Figure 9.** Average RMSE of Lorenz'63 system for ensemble size  $N = 400$  as a function of observation interval (Left), and for observation interval  $\Delta t_{ob} = 0.5$  as a function of ensemble size (Right).

EnTranF(L-G) have 25.30% and 18.63% improvement on RMSE, respectively, when taking observation interval as  $\Delta t_{ob} = 0.5$ . A well-chosen kernel function can make EnTranF more robust in systems with strong nonlinearity. The right panel of Figure 9 shows the average RMSE of EnTranF as a function of ensemble size for the observation interval to be fixed. Since the EnTranF is based on Particle Filter, it exhibits almost no advantage over EnKF and may even perform worse when the ensemble size is small ( $N < 20$ ). However, EnTranF performs better than EnKF in the filtering problem of the Lorenz'63 system at larger aggregate ensemble sizes. If ensemble size  $N \geq 100$ , EnTranF(L-G) has about 18.56% improvement on average RMSE compared to EnKF, and EnTranF(N-G) has about 25.04% improvement. Unlike the one-dimensional double-well problem, the EnTranF with a nonlinear transport map has apparent advantages over the linear version. The relatively higher dimensional Lorenz'63 system exhibits strong nonlinearities in partial observations, making methods based on linear transport maps less effective.

The ensemble spread of different filtering methods is shown in Figure 10. EnTranF(N-G) reduces the ensemble spread compared to EnTranF(L-G). However, both EnTranF(N-G) and EnTranF(L-G) have a larger ensemble spread with different observation intervals and ensemble sizes. This may be caused by inadequate optimization of the MMD loss function. EnTranF fails to approximate the posterior adequately. The EnTranF with a variance penalty can significantly improve the spread and slightly improve the average RMSE. Figure 11 and Figure 12 respectively depict the average RMSE and Spread versus a range of observation intervals and ensemble sizes.

The average RMSE of EnTranF with a variance penalty outperforms EnKF at different observation intervals (see left panel of Figure 11). After introducing the variance penalty term, even EnTranFp with a linear kernel function shows a significant performance improvement on average RMSE compared to EnKF. EnTranF(L-L) has 14.20% improvement, and EnTranF(N-L) has 23.57% improvement. EnTranFp also shows some improvement compared to EnTranF when taking a Gaussian kernel func-

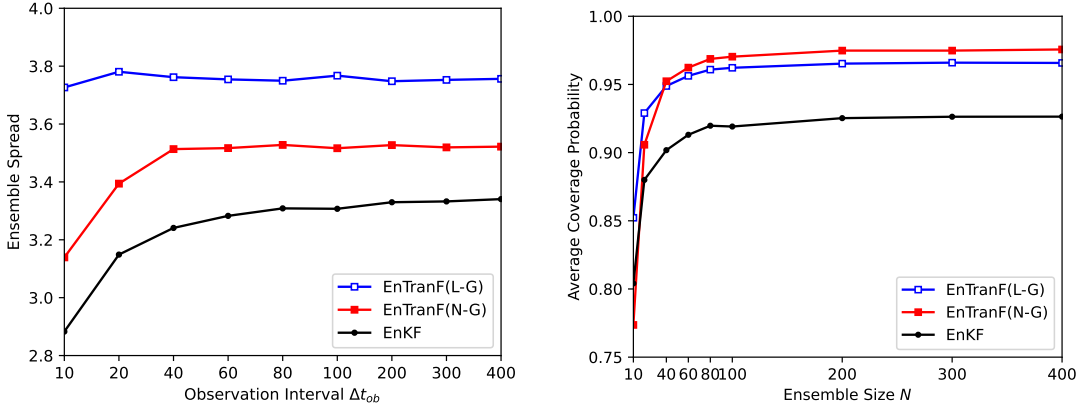


**Figure 10.** Spread of Lorenz'63 system for ensemble size  $N = 400$  as a function of observation interval (Left), and for observation interval  $\Delta t_{ob} = 0.5$  as a function of ensemble size (Right).

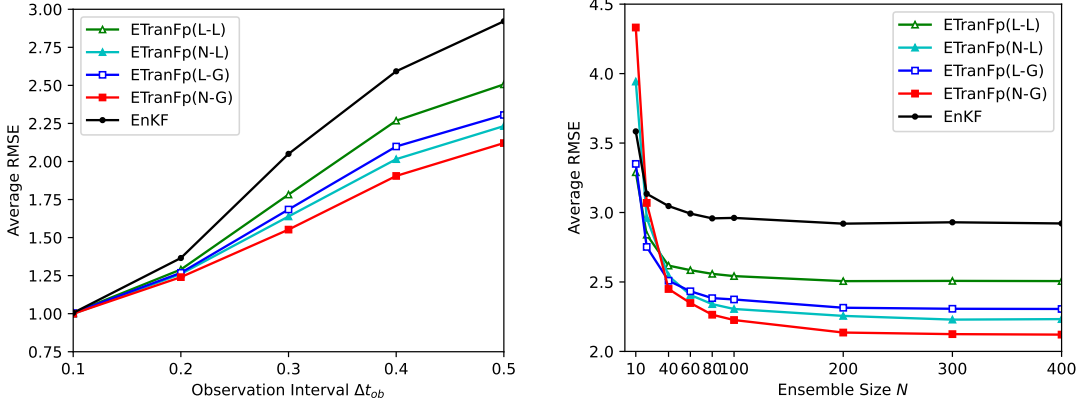


**Figure 11.** *EnTranF* with variance penalty: Average RMSE of Lorenz'63 system for ensemble size  $N = 400$  as a function of observation interval (Left), and for observation interval  $\Delta t_{ob} = 0.5$  as a function of ensemble size (Right).

tion. Here, EnTranFp(L-G) is 21.07% better than EnKF on RMSE at observation interval  $\Delta t_{ob} = 0.5$ , while EnTranFp(N-G) is 27.39% better than EnKF. From panel (b) of Figure 11, EnTranFp has a smaller average RMSE when  $N \geq 20$  than EnKF for different ensemble sizes. In Figure 12, EnTranFp(L-L), EnTranFp(N-L), and EnTranFp(L-G) show a similar spread to EnKF but get a higher probability of covering the true state. EnTranFp(N-G) performs optimally in the Lorenz63 system. It significantly reduces the spread while maintaining a high probability of covering the true state. The variance penalty term effectively guides EnTranF in prioritizing the approximation of high-informative statistics of the posterior distribution. It enhances the robustness of EnTranF in high-dimensional nonlinear systems.

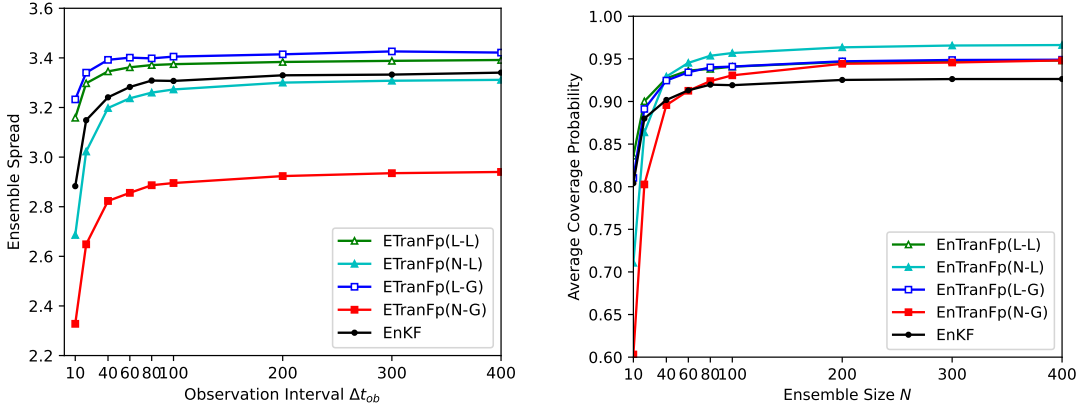


**Figure 12.** *EnTranF with variance penalty: Spread of Lorenz'63 system for ensemble size  $N = 400$  as a function of observation interval (Left), and for observation interval  $\Delta t_{ob} = 0.5$  as a function of ensemble size (Right).*

**4.4. Lorenz'96 System.** The Lorenz96 model is a simplified mathematical model that describes the nonlinear dynamical behavior in atmospheric circulation systems. It consists of a set of coupled one-dimensional differential equations, each representing a grid point within the atmospheric circulation system. These differential equations are typically given by:

$$(4.7) \quad \frac{dX_i}{dt} = (X_{i+1} - X_{i-2})X_{i-1} - X_i + F.$$

Here,  $X_i$  represents the state variable at the  $i$ -th grid point, and  $F$  is an external forcing.

The numerical example is conducted to evaluate the performance of EnTranF for a of Lorenz'96 system in which sparse observations are given both in space and time. We take 20-dimension state variables and observe 10 dimensions of them (observing every other state component). We simulate the ODEs (4.7) by using a fourth-order Runge-Kutta method with time stepsize  $\Delta t = 0.01$ . The observation interval in time is set to be  $\Delta_{ob} = 0.1$ . Results of EnTranF(N-G) are presented in Figure 13 and Figure 14. From Figure 13, EnTranF(N-G) successfully achieves the estimation of the Lorenz96 state, with error performance similar to that of EnKF. Panel (a) and Panel (b) of Figure 14 respectively present the RMSE and Spread of EnTranF(N-G) and EnKF. We note that EnTranF(N-G) is comparable to EnKF in RMSE and the spread.

**5. Conclusion.** In this paper, we reconstructed the analysis step of the particle filter through a transport map, which directly transported the prior particles to the posterior particles. By matching the expectation information of posterior distribution, the problem was converted into an optimization problem for the Maximum Mean Discrepancy loss function. In the ensemble transport filter, the particle weights in the analysis step of the particle filter were substituted with the update of particle states, effectively alleviating the risk of particle degeneracy in high-dimensional problems. Meanwhile, the



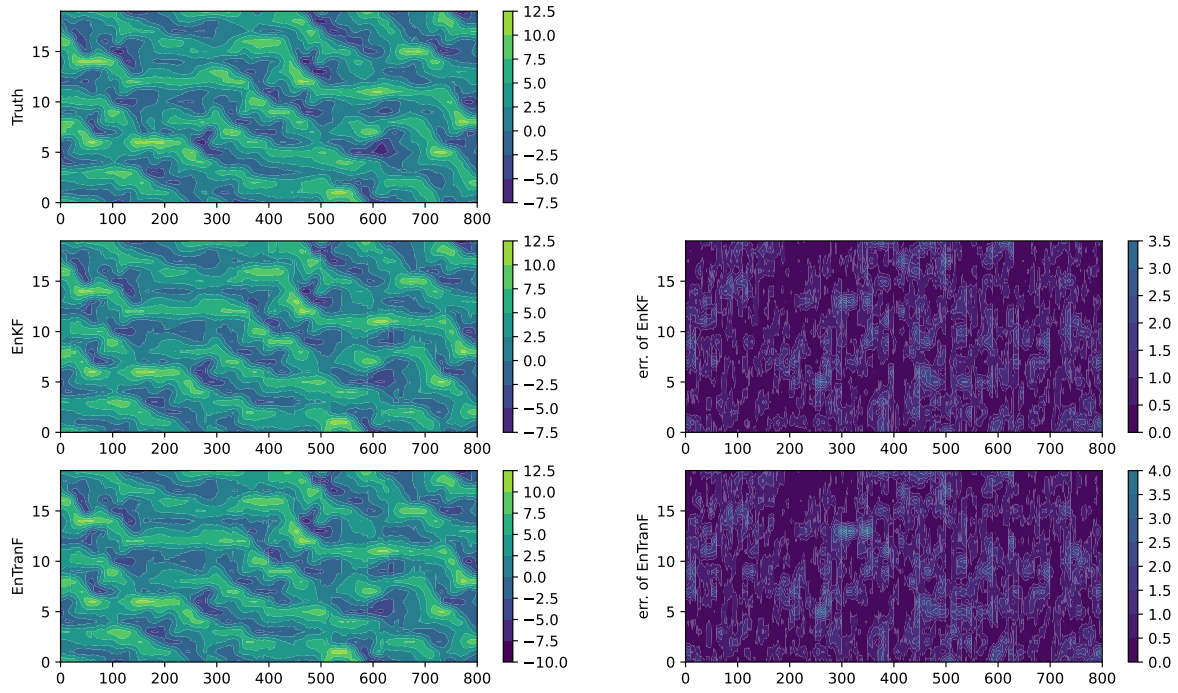


**Figure 13.** State estimation and absolute error of Lorenz'96 system for observation interval  $\Delta t_{ob} = 0.1$  and ensemble size  $N = 2000$ .

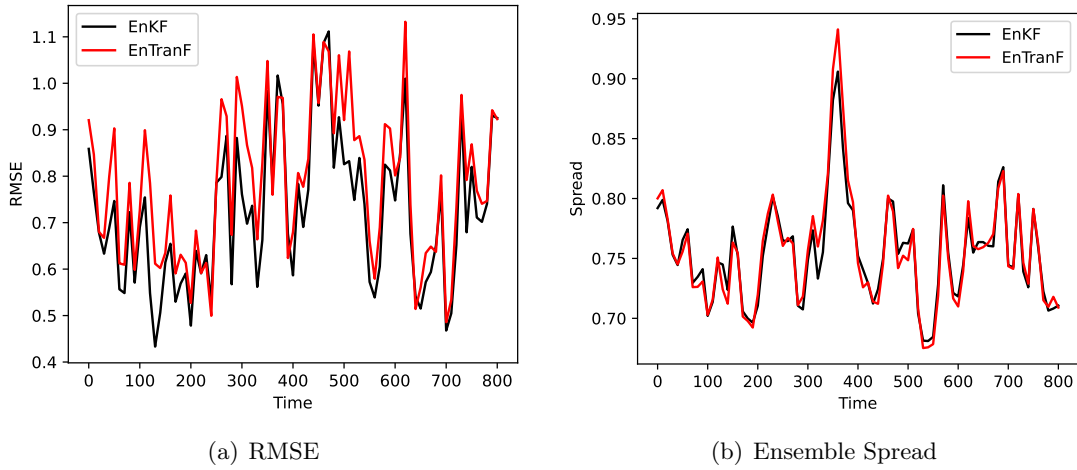


**Figure 14.** RMSE and Spread of Lorenz96 system for observation interval  $\Delta t_{ob} = 0.1$  and ensemble size  $N = 2000$ .

ensemble transport filter inherited the accurate estimation of the posterior distribution from the particle filter. To improve the robustness of MMD, we introduced a variance penalty term to guide the prioritized optimization of high-informative statistics in the

approximate posterior and reference posterior.

Numerical results demonstrated that the ensemble transport filter outperformed EnKF significantly in lower-dimensional problems, particularly in strongly nonlinear systems. The ensemble transport filter remained stable in high-dimensional systems and performed comparably to EnKF. The variance penalty term effectively enhanced the robustness of our method in approximating the filtering posterior, making it more effective and stable. EnTranF with a variance penalty term significantly reduced the spread of ensemble methods while maintaining RMSE.

The general transport map structure can be explored for future work to avoid computationally expensive optimization problems when constructing the transport map at each assimilation window.

## REFERENCES

- [1] J. BRAJARD, A. CARRASSI, M. BOCQUET, AND L. BERTINO, *Combining data assimilation and machine learning to infer unresolved scale parametrization*, Philosophical Transactions of the Royal Society A: Mathematical, Physical and Engineering Sciences, 379 (2021), p. 20200086.
- [2] A. CARRASSI, M. BOCQUET, L. BERTINO, AND G. EVENSEN, *Data assimilation in the geosciences: An overview of methods, issues, and perspectives*, WIREs Climate Change, 9 (2018), p. e535.
- [3] A. CHATTOPADHYAY, E. NABIZADEH, E. BACH, AND P. HASSANZADEH, *Deep learning-enhanced ensemble-based data assimilation for high-dimensional nonlinear dynamical systems*, Journal of Computational Physics, 477 (2023), p. 111918.
- [4] A. J. CHORIN AND X. TU, *Implicit sampling for particle filters*, Proceedings of the National Academy of Sciences, 106 (2009), pp. 17249–17254.
- [5] T. A. EL MOSELHY AND Y. M. MARZOUK, *Bayesian inference with optimal maps*, Journal of Computational Physics, 231 (2012), pp. 7815–7850.
- [6] G. EVENSEN, *The ensemble kalman filter: Theoretical formulation and practical implementation*, Ocean Dynamics, 53 (2003), pp. 343–367.
- [7] G. EVENSEN, *Sampling strategies and square root analysis schemes for the enkf*, Ocean Dynamics, 54 (2004), pp. 539–560.
- [8] G. EVENSEN, *The ensemble kalman filter for combined state and parameter estimation*, IEEE Control Systems, 29 (2009), pp. 83–104.
- [9] A. FARCHI AND M. BOCQUET, *Review article: Comparison of local particle filters and new implementations*, Nonlinear Processes in Geophysics, 25 (2018), pp. 765–807.
- [10] A. FARCHI, P. LALOYLAUX, M. BONAVITA, AND M. BOCQUET, *Using machine learning to correct model error in data assimilation and forecast applications*, Quarterly Journal of the Royal Meteorological Society, 147 (2021), pp. 3067–3084.
- [11] A. GRETTON, K. BORGWARDT, M. RASCH, B. SCHÖLKOPF, AND A. SMOLA, *A kernel method for the two-sample-problem*, in Advances in Neural Information Processing Systems, vol. 19, MIT Press, 2006.
- [12] D. J. HIGHAM., *An algorithmic introduction to numerical simulation of stochastic differential equations*, SIAM Review, 43 (2001), pp. 525–546.
- [13] T.-V. HOANG, S. KRUMSCHEID, H. G. MATTHIES, AND R. TEMPONE, *Machine learning-based conditional mean filter: A generalization of the ensemble kalman filter for nonlinear data assimilation*, Foundations of Data Science, 5 (2023), pp. 56–80.
- [14] L. JIANG AND N. LIU, *Correcting noisy dynamic mode decomposition with kalman filters*, Journal of Computational Physics, 461 (2022), p. 111175.
- [15] T. KAWABATA AND G. UENO, *Non-gaussian probability densities of convection initiation and development investigated using a particle filter with a storm-scale numerical weather prediction model*, Monthly Weather Review, 148 (2020), pp. 3–20.

- [16] K. LAW, A. STUART, AND K. ZYGALAKIS, *Data Assimilation: A Mathematical Introduction*, no. volume 62 in Texts in Applied Mathematics, Springer, Cham Heidelberg New York Dordrecht London, 2015.
- [17] R. S. LIPTSER AND A. N. SHIRYAEV, *Statistics of Random Processes II: Applications*, vol. 6 of Stochastic Modelling and Applied Probability, Springer Berlin Heidelberg, Berlin, Heidelberg, 2001.
- [18] R. S. LIPTSER AND A. N. SHIRYAYEV, *Statistics of Random Processes I: General Theory*, Springer New York, New York, NY, 1977.
- [19] N. LIU AND L. JIANG, *Perron–frobenius operator filter for stochastic dynamical systems*, SIAM/ASA Journal on Uncertainty Quantification, 12 (2024), pp. 182–211.
- [20] A. J. MAJDA AND J. HARLIM, *Filtering Complex Turbulent Systems*, Cambridge University Press, 1 ed., Feb. 2012.
- [21] J. MANDEL, L. COBB, AND J. D. BEEZLEY, *On the convergence of the ensemble kalman filter*, Applications of Mathematics, 56 (2011), pp. 533–541.
- [22] G. MONGE, *Mémoire sur la théorie des déblais et des remblais*, Mem. Math. Phys. Acad. Royale Sci., (1781), pp. 666–704.
- [23] M. PULIDO AND P. J. VAN LEEUWEN, *Sequential monte carlo with kernel embedded mappings: The mapping particle filter*, Journal of Computational Physics, 396 (2019), pp. 400–415.
- [24] A. RAMDAS, S. JAKKAM REDDI, B. POCZOS, A. SINGH, AND L. WASSERMAN, *On the decreasing power of kernel and distance based nonparametric hypothesis tests in high dimensions*, Proceedings of the AAAI Conference on Artificial Intelligence, 29 (2015).
- [25] P. REBESCHINI AND R. VAN HANDEL, *Can local particle filters beat the curse of dimensionality?*, The Annals of Applied Probability, 25 (2015).
- [26] D. RICHARD M, *Real Analysis and Probability*, Chapman and Hall/CRC, 2002.
- [27] P. SAKOV, D. S. OLIVER, AND L. BERTINO, *An iterative enkf for strongly nonlinear systems*, Monthly Weather Review, 140 (2012), pp. 1988–2004.
- [28] A. SPANTINI, R. BAPTISTA, AND Y. MARZOUK, *Coupling techniques for nonlinear ensemble filtering*, SIAM Review, 64 (2022), pp. 921–953.
- [29] P. J. VAN LEEUWEN, *Particle filtering in geophysical systems*, Monthly Weather Review, 137 (2009), pp. 4089–4114.
- [30] C. VILLANI, *Optimal Transport: Old and New*, vol. 338 of Grundlehren Der Mathematischen Wissenschaften, Springer Berlin Heidelberg, Berlin, Heidelberg, 2009.
- [31] Z. WANG, W. XING, R. KIRBY, AND S. ZHE, *Physics informed deep kernel learning*, in Proceedings of The 25th International Conference on Artificial Intelligence and Statistics, PMLR, May 2022, pp. 1206–1218.
- [32] H. YAN, Z. LI, Q. WANG, P. LI, Y. XU, AND W. ZUO, *Weighted and class-specific maximum mean discrepancy for unsupervised domain adaptation*, IEEE Transactions on Multimedia, 22 (2020), pp. 2420–2433.
- [33] S. ZHANG, Z. LIU, X. ZHANG, X. WU, G. HAN, Y. ZHAO, X. YU, C. LIU, Y. LIU, S. WU, F. LU, M. LI, AND X. DENG, *Coupled data assimilation and parameter estimation in coupled ocean–atmosphere models: A review*, Climate Dynamics, 54 (2020), pp. 5127–5144.
- [34] M. ZHU, P. J. VAN LEEUWEN, AND J. AMEZCUA, *Implicit equal-weights particle filter*, Quarterly Journal of the Royal Meteorological Society, 142 (2016), pp. 1904–1919.